Workshop I

VLBI for Astronomy and Geodynamics

Chairman:
Prof. Leonid Litvinenko (IRA NASU, Ukraine)

Session 1. VLBI for Astronomy

Convener: Dr. Chopo Ma (NASA GSFC, USA)

RATAN-600 AND EVN OBSERVATIONS OF QUASAR 0642+449

A. E. Volvach[1], N. S. Nesterov[1], and M. G. Mingaliev[2]

[1] *Crimean Astrophysical Observatory, RT-22, Katsiveli, 98688 Crimea, Ukraine*
e-mail: `volvach@crao.crimea.ua`
[2] *Special Astrophysical Observatory, Nizhny Arkhyz, Karachaevo-Cherkessia, 357147 Russia*

Observational results for the high redshift quasar OH 471 obtained by means of RATAN-600 in March and May 1998 at 0.96, 2.3, 3.9, 7.7, 11.2, 21.7 GHz are presented. The radio spectrum of source has a peak at about 20 GHz.
We present 1.6 GHz EVN observations of OH 471. Our VLBI data showed that 0642+449 has an extended structure like core-jet. The jet was elongated for about 5 mas to the East. The flux density of the core component was 0.328 Jy.

1. INTRODUCTION

The OH 471 radio source coincides with the highly redshifted QSO having $z = 3.4$ (Carswell and Strittmatter, 1973). Gearhart *et al.* (1974) determined its radio spectrum in wide frequency range from 16.7 MHz up to 85.3 GHz and pointed out possible day to day variability at high radio frequencies. According to their study the OH 471 radio source had radio spectrum peaked at about 1 GHz and flatted at frequencies above 5 GHz in 1970–1973. Jones and O'Dell (1974) decomposed this spectrum into three hypothetical homogeneous synchrotron components and predicted angular size of about 2 mas for component dominated at frequencies below 5 GHz.

Several years later Efanov *et al.* (1980, 1981) found distinctly that at the beginning of 1978 this quasar had a strong millimeter wave spectral component and showed that it is actually variable at 22 GHz. Optical monitoring in photographical band by Pica *et al.* (1980) revealed a high probability that QSO is variable in this part of spectrum too.

In this paper we present RATAN-600 and EVN observations of OH 471.

2. THE SAMPLE

Table 1 shows parameters of source. Column (1) shows IAU source designation, Columns (2) and (3) are right ascension and declination (J2000), Column (4) is optical magnitude, Column (5) is redshift.

Table 1: Source parameters[(1)]

Source	RA (J2000) (^{h})	(^{m})	(^{s})	Dec (J2000) ($^\circ$)	($'$)	($''$)	Optical magnitude	z
0642+449	06	46	32.026	+44	51	16.590	18.5	3.41

[(1)] according to Kellermann *et al.*, 1998

RATAN-600 and 1.6 GHz VLBI observations is a part of program of investigation of the spectrum and structure of the source. In accordance with this program we have completed:

– observations on 22-m radio telescope of Crimean Astrophysical Observatory at 22 and 37 GHz (since 1973);

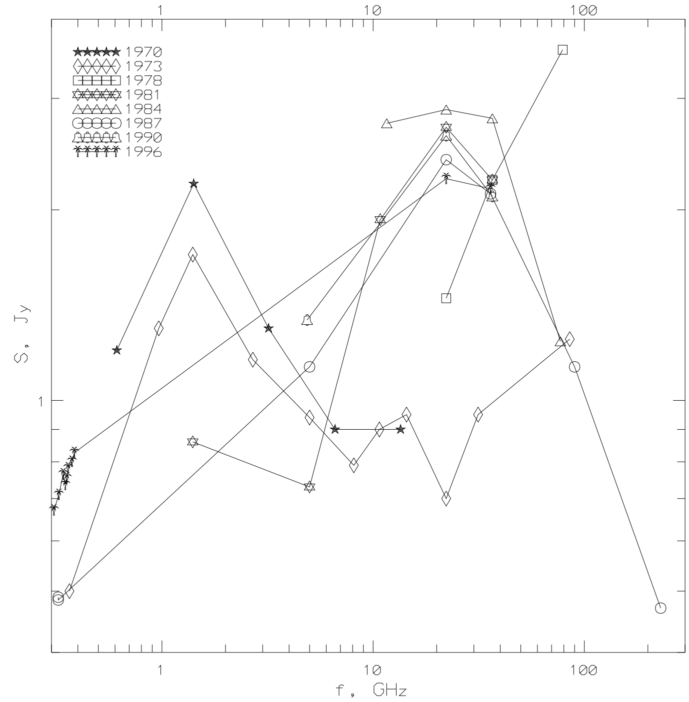

Figure 1: The radio spectra OH 471 for several epochs

– observations on the Westerbork radio telescope of aperture syntheses (WSRT) at 307–385 MHz (in 1996);
– the re-processing data from the WSRT archive at 307–385 MHz and 4874 MHz (completed in 1987–1990);
– the processing data on this source at other frequencies (published since 1964).

Figure 1 shows OH 471 radio spectra for several epochs since 1970 (Nesterov *et al.*, 2000).

3. OBSERVATIONS, CALIBRATION AND DATA REDUCTION

3.1. RATAN-600

The observations were made at 21.7 GHz, 11.2 GHz, 7.7 GHz, 3.9 GHz, 2.3 GHz, and 0.96 GHz by transit way mode at the North sector of the RATAN-600 radio telescope (Berlin *et al.*, 1997; Parijskij, 1997). We have used two strong radio sources NGC 7027 and DR21 as a flux standard. The assumed flux densities for NGC 7027 are following: 5.5 Jy, 6.02 Jy, 6.33 Jy, 5.0 Jy, and 2.6 Jy at 21.7 GHz, 11.2 GHz, 7.7 GHz, 3.9 GHz, and 2.3 GHz, respectively; and for DR21 5.0 Jy at 0.96 GHz. The correction factor due to an angular extension of NGC 7027 and beam size were calculated at 7.7, 11.2 and 21.7 GHz. Each scan was corrected for baseline slope when fitted to Gaussian response using FGR data reduction software developed by Verkhodanov (1997). The accuracy of flux densities was determined as the standard error of the mean value from N observations of a set. The flux density measurement procedure at the RATAN-600 is described by Aliakberov *et al.* (1985) in more detail.

The flux densities measured at the RATAN-600 are given in Table 2. The columns in this table are following: Column (1) – Frequency of observations, Column (2) and Column (3) – Flux densities and the rms errors of the flux densities measured in March and May.

Table 2: RATAN-600 measured flux densities of OH 471

	March		May	
Freq (GHz)	Flux (mJy)	rms (mJy)	Flux (mJy)	rms (mJy)
0.96	–	–	173	17
2.3	630	13	597	14
3.9	1483	16	1465	11
7.7	2516	13	2540	13
11.2	2710	84	2958	25
21.7	2807	80	3099	111

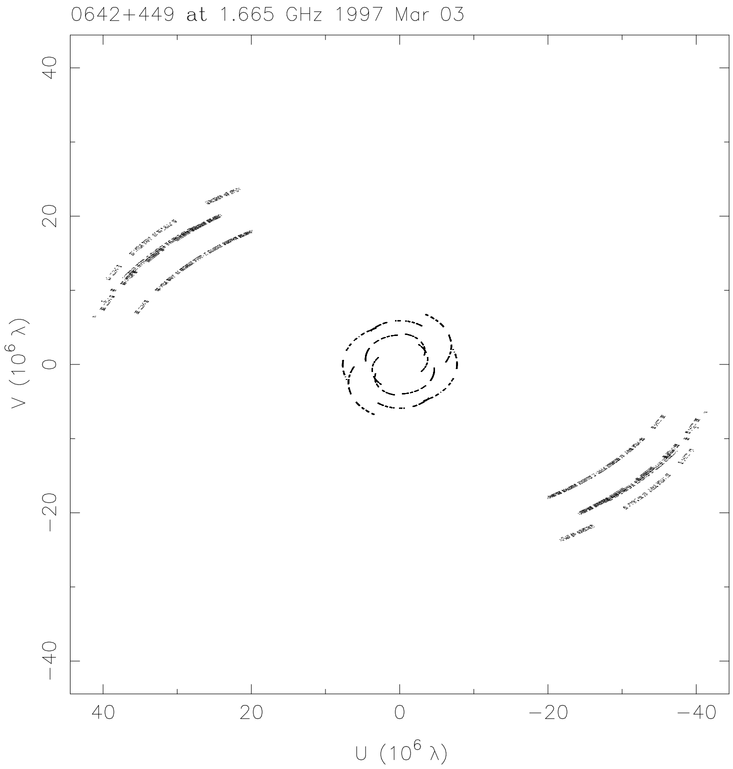

Figure 2: The $u-v$ coverage ENV observations of OH 471

3.2. EVN NETWORK

The source 0642+449 was observed in left circular polarization at 1.6 GHz in EVN session in 1997 (see Table 3).

Table 3: VLBI telescopes experiment and their characteristics at 1.6 GHz (March, 1997)

Radio telescope	Diameter (m)	SEFD[a] (Jy)
Effelsberg	100	20
Medicina	32	580
Onsala	25	390
Jodrell Mk2	26	320
Torun	32	200
Shanghai	25	2000

[a] System Equivalent Flux Density

The data were recorded using the Mark-III VLBI system and correlated at the Bonn correlator. In Figure 2 we show the $u-v$ coverage for the source.

Initial editing, amplitude calibration using the nominal gain curves determined for each antenna, and fringe fitting were performed using the standard NRAO Astronomical Image Processing System (AIPS) package. The initial amplitude calibration for each of eight IFs was accomplished using system temperature measurements taken during the observations. After correction for residual delay and delay rate, the data were written to FITS disk files.

The amplitude calibration was improved by observations of the 0552+398 (DA193) and 1328+307 (3C286) compact sources. The visibility data for each frequency band were selfcalibrated and cleaned using DIFMAP.

DISCUSSION

Correlated flux density (Jy) versus projected baseline length for 0642+449 (Fig. 3) shows a gradual drop in amplitude as the projected baseline length increases, indicative of slightly resolved structure. Our VLBI data

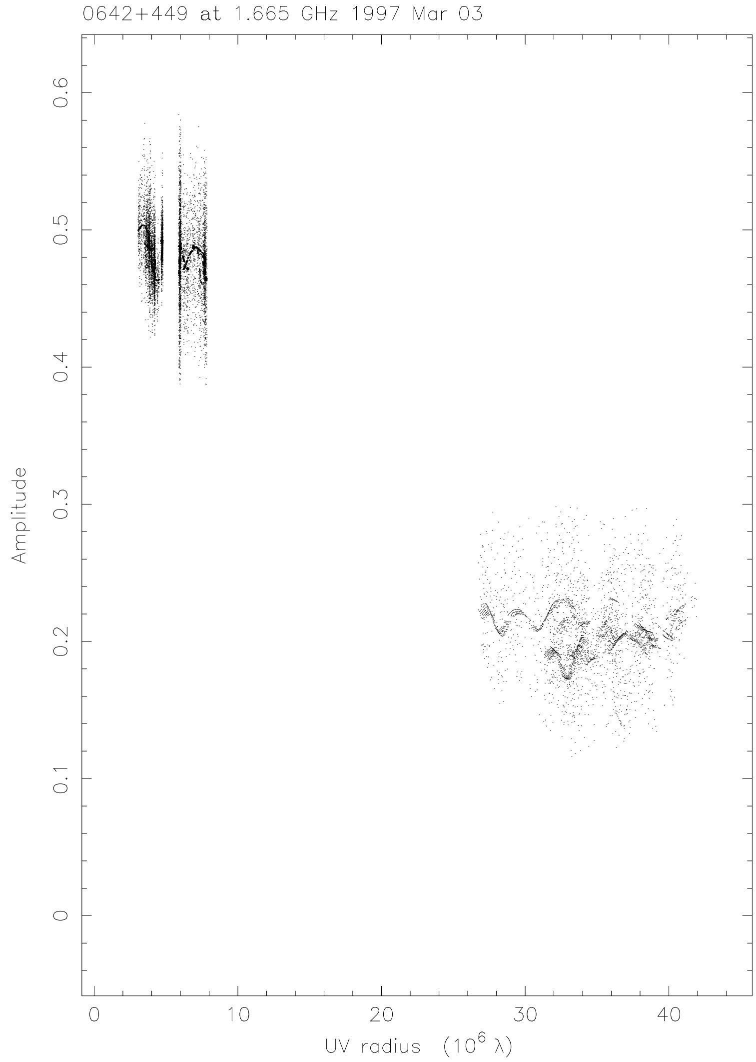

Figure 3: Correlated flux density versus projected baseline length for 0642+449

show that slightly resolved structure of 0642+449 has an extended structure like core-jet. The jet is elongated for about 5 mas to the east. The flux density of the core component is equal to 0.328 Jy.

Our VLBI observations have a very elongated beam (HPBW=12.8×2.55 mas) oriented in position angle of −24°. It would slightly mask a compact structure on VLBI scales which may be aligned with the arcsec scale structure.

It was found that at the beginning of 1970s the spectrum of OH 471 had a peak at frequencies near 1 GHz (see Fig. 1). The spectrum at frequencies above 5-10 GHz was always flatter than at lower frequencies. In Figure 4 we show 1–22 GHz spectra of OH 471 for 1998 epoch obtained at the RATAN-600. Our measurements at the RATAN-600 overlay a gap in low frequency observations of OH 471 for the 1980–1996 period. It is apparent that in 1998 the spectrum of source had peak at frequencies near 20 GHz. The apparent spectrum variability is attributed to the birth and the fading of new compact jet components.

CONCLUSION

The radio spectrum of OH 471 had a peak at about 20 GHz according to the RATAN-600 observations completed in 1998.

Our VLBI data showed that slightly resolved structure of source has an extended structure like core-jet, which is in agreement with earlier VLBI observations. The jet was elongated for about 5 mas to the East. The flux density of the core component was equal to 0.328 Jy.

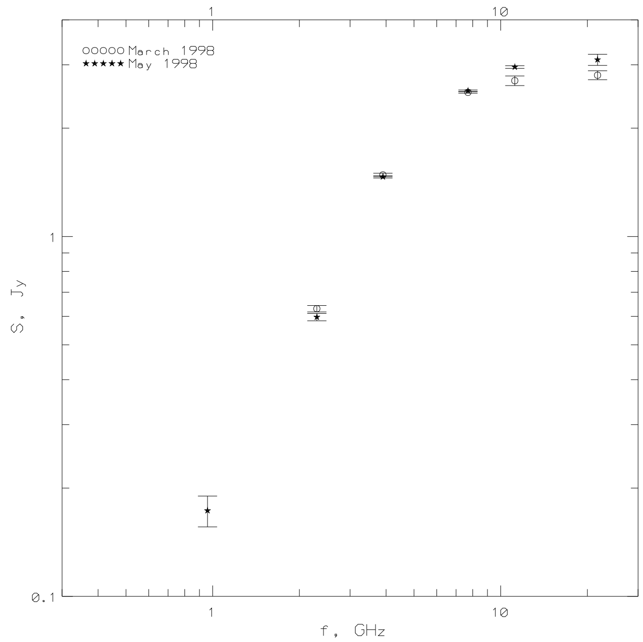

Figure 4: 1–22 GHz spectra of OH 471

Acknowledgments. We are grateful to the staff of the RATAN-600, the EVN observatories, the staff of MPIfR correlator and the JIVE for their support of our project.

REFERENCES

[1] *Aliakberov K., Mingaliev M., Naugol'naya M., et al.* // Astrophys. Issled. (Izvestiya SAO).–1985–**19**.–P. 60. (in Russian).

[2] *Berlin A., Maksyasheva A., Nizhelskij N., et al.* // The problems of Modern Radio Astronomy: 27th Radio Astron. Conf.–Saint-Petersburg, 1997.–P. 115.

[3] *Carswell R. F. and Strittmatter P. A.* // Nature.–1973.–**242**.–P. 396.

[4] *Efanov V. A., et al.* // Pisma v Astron. Zh.–1980.–**6**.–P. 340. (in Russian).

[5] *Efanov V. A., et al.* // Izv. Krymskoy Astr. Obs.–1981.–**54**.–P. 103. (in Russian).

[6] *Gearhart M. R., Kraus J. D., Andrew B. H., et al.* // Nature.–1974.–**249**.–P. 743–746.

[7] *Jones T. W., O'Dell S. L.* // Nature.–1974.–**250**.–P. 472–474.

[8] *Kellerman K. I., Vermeulen R. C., Zensus J. A., Cohen M. H.* // Astron. J.–1998.–**115**.–P. 1295–1318.

[9] *Korolkov D. V., Parijskij Yu. N.* // Sky and Telesc.–1979.–**57**.–P. 324.

[10] *Nesterov N. S., Volvach A. E., Pogrebenko S. V.* // Astron. Lett.–2000.–submitted.

[11] *Parijskij Yu.* // IEEE Antennas and Propagation Magazine.–1997.–**35**.–P. 7.

[12] *Pica A. J., Pollock J. T., Smith A. G., et al.* // Astron. J.–1980.–**85**, N 11.–P. 1442–1461.

[13] *Verkhodanov O.* // Astronomical Data Analysis Software and Systems VI: ASP Conf. Ser. / Eds G. Hunt, H. E. Payne.–1997.–**125**.–P. 46.

IR/RADIO QUASARS FOR VLBI AND INFRARED POSITIONAL OBSERVATIONS

A. S. Kharin

Main Astronomical Observatory, NAS of Ukraine
27 Akademika Zabolotnoho St., 03680 Kyiv, Ukraine
e-mail: kharin@mao.kiev.ua

A search for the ICRF radio sources that have been also observed in infrared frequency region have been undertaken. The comparison of the list of 179 quasars observed by IRAS satellite in 1983 [8] with the ICRF list of 608 radio sources [7] has been carried out and 55 common extragalactic sources were found.

INTRODUCTION

Precise enough positional observations in infrared (IR) are absent. CPIRSS, the Catalog Point Infrared Stellar Sources, is not proper usual observational catalogue. It was compiled by the way of IR/Optics counterparts identifications. The 37700 IR/Optics objects of this catalogue, which have been identified with their optical counterparts from five precise astrometric catalogues [3] are IR sources from the IRAS Point Source Catalog (PSC) [1].

In accordance with our conception [5], the CPIRSS was transformed and two level hierarchic IR reference coordinate system was created [6]. The first level IR reference catalogue includes only IR stars, which have their optical counterparts from HIPPARCOS and, therefore, it represents the ICRS coordinate system. However, the best representation of this system can be obtained if this first level IR reference catalogue will include additionally the ICRF sources that could be observed in infrared as well.

Because of this point of view an research has been undertaken to find the ICRF radio sources that were observed in infrared too. The list of 179 quasars observed by IRAS satellite in 1983 [8] and two published versions of the ICRF were used for this purpose.

Finally the comparison of the above list of 179 quasars with the ICRF list of 608 candidate sources [7] has been carried out and 55 common IR/Radio extragalactic sources were found.

CHARACTERIZATION AND COMPARISON OF TWO ICRF LISTS

International Celestial Reference Frame (ICRF) is a realization of the new International Celestial Reference System (ICRS) that has replaced from January 1, 1998 the previous coordinate system based on the FK5 Fundamental Catalogue. The list of candidate sources that has to define ICRF has two versions. The first preliminary one was prepared by IAU/WG IERS and presented to XXII IAU GA in Hague in September 1994. It was published in [9].

This list includes 606 objects which are divided into three different sorts of sources, namely d – defining sources, c – additional sources and o – optical sources. The quantitative distribution between these three categories is presented in Table 1.

Table 1: The ICRF list of 606 sources and its identification

Objects	**ICRF606**	**IRAS179/ICRF606**
d – defining sources	441	46
c – additional sources	92	4
o – optical objects	73	4
All	606	54

Besides of d, c, o classification the above mentioned list contains: IERS designation constructed from B1950 coordinates; R.A. and Dec. with $0\overset{s}{.}01$ and $0\overset{''}{.}1$ accuracy accordingly; alias names for all sources which have such ones.

A final version of the ICRF list was prepared also by the IAU/WG IERS. It has been presented to XXIII IAU GA in Tokyo in September 1997 and adopted as new conventional celestial reference frame.

This list also consists of three files. The first one has the same name "defining sources" but the second and third files have some other names: "candidate" and "other" accordingly. Besides, they have some other interpretation and an other quantitative distribution presented in Table 2.

Table 2: The ICRF list of 608 sources and its identification

Objects	**ICRF608**	**IRAS179/ICRF608**
d – defining sources	212	17
c – candidate sources	294	23
o – "other" sources	102	15
All	608	55

There are only 212 "defining sources", 294 – "candidates" and 102 – "others". But in this case there is more strong file classification in comparison with the first list version. It is result of strong solving equations of condition formed here on the base of the VLBI and precise optical observations [7].

The final list contains 608 objects and first one – 606, but there is more big difference between them. To transit from the first list to the final one 56 objects had to be excluded and 58 new ones be included. The IAU/WG IERS carried out a very vast work to create final ICRF list version.

BRIEF DESCRIPTION OF THE IRAS 179 QUASAR LIST

The list of 179 more bright quasars [8] was compiled on the base of the second IRAS programme that was named "Point observations". It was carried out apart from the main "All sky survey" IRAS programme which has been used to create PSC. Quantitative spectral distribution of 179 bright quasar catalogue is presented in Table 3.

Table 3: Astrophysical characteristics of the IRAS 179 quasars

Quasartypes	**IRAS179**	**IRAS179/ICRF608**
F – flat radio spectrum	56	42
S – steep radio spectrum	34	4
I – intermediate radio sp.	22	8
Q – radio quiet	67	1
All	179	55

As one can see, a catalogue of 179 bright quasars contains 56 sources with flat radio spectrum, 34 – with steep, 22 – with intermediate radio spectrum, and 67 sources are the radio quiet quasars[1].

IRAS(179)/ICRF(606) AND IRAS(179)/ICRF(608) CROSS-IDENTIFICATIONS

The IRAS 179 quasars catalog does not contain equatorial coordinates and has only B1950 identificator. Therefore, its cross-identifications with first and final versions of ICRF list were carried out by using only these identificator. The accuracy of such identification is not high but the errors may not exceed $7\overset{'}{.}5$ in R.A. and $3'$ in Declination. Such identification has to be qualified as preliminary one and its verification is still necessary.

As results of the first IRAS(179)/ICRF(606) and the second IRAS(179)/ICRF(608) identifications, the lists of 54 and 55 quasars were obtained. 52 quasars are common of both the first and the second ones. The distributions in relation of files classification are presented in Tables 1 and 2, and one can see that first list has a much better relation (46:4:4) in comparison with the second one (17:23:15). But only the second list of 55 common IR/ICRF sources obtained as the result of IRAS 179 quasars and ICRF 608 radio sources identifications was used for further operation. It is presented in Table 4.

[1]The quasars are named "radio quiet" if their luminosity at 6 cm is less than $10^7 L_\odot$.

Table 4: Flux densities of 55 common IRAS 179/ICRF 608 quasar for 12, 25, 60, and 100 μm bands in μJa

N	$ICRF(J2000)$	$B1950$	[12]		[25]		[60]		[100]		$L_{60}/L_{\odot}$	REM
1d	1031.0+105829	0007+106	99	± 6	163	±12	213	± 8	845		10.64	F,2
2o	13741.2+330935	0134+329	56	± 6	160	± 8	770	± 9	1080	±27	12.52	S
3c	20457.6-170119	0202-172	41		61		82	±21	200		12.98	F,3
4d	20504.9+321230	0202+319	20		32		30		87		12.37	F
5c	23145.8+132254	0229+131	20		45		26		79		12.65	I
6c	23752.4+284808	0234+285	35		65		187	±18	178		12.98	F,2
7c	31155.2-765150	0312-770	37		38		62		194		10.92	F
8o	33630.1+321829	0333+321	36		64		97		874		12.74	F
9c	35721.9-481215	0355-483	41		44		78		273		12.44	I
10d	40305.5+260001	0400+258	40		79		57		277		13.01	F,5
11c	40748.4-121136	0405-123	87		116	±31	126		312		12.10	F,5
12o	42315.8-012033	0420-014	25	±10	92	±17	271	±16	565	±61	12.96	I
13d	42442.2-375620	0422-380	31		36		50		158		12.00	F
14c	44017.1-433308	0438-436	25	± 8	28		120	±14	279	±47	13.62	F
15d	50643.9-610940	0506-612	26		29		48		155	±52	12.29	F
16o	53850.3-440508	0537-441	149	±10	298	±11	631	±25	808	±91	13.14	F
17c	60940.9-154240	0607-157	25		34		54	±13	147		11.20	F,3
18d	64632.0+445116	0642+449	34		51		51		155		13.42	S,2
19o	71424.8+353439	0711+356	19		33	±11	28	±9	87		12.44	F
20c	73918.0+013704	0736+017	34	± 6	77	± 9	133	± 8	564		11.11	F,3
21d	74110.7+311200	0738+313	20		39		145	± 9	282		12.25	F,3
22c	74331.6-672625	0743-673	39		41		66		245		12.74	S
23c	75052.0+123104	0748+126	37		67		205	±17	365	±51	12.73	F
24o	92703.0+390220	0923+392	15		26		27		80		11.61	F
25c	110331.5-325116	1101-325	39		52		67		225		11.38	F
26c	111826.9-463415	1116-462	41		48		86		335		12.14	I
27d	114608.1-244732	1143-245	55		78		79		247		13.07	F
28c	115043.8-002354	1148-001	45		86		64		200		12.99	F
29d	115324.4+493108	1150+497	21	± 6	25	± 7	42	±11	108		11.12	I
30c	115931.8+291443	1156+295	20		33	±11	126		85		12.33	I,8
31c	120935.2-401613	1206-399	39		55		64		404	±68	12.30	F
32o	122906.6+020308	1226+023	417	±12	941	±27	1805	±14	3109	±45	12.07	F
33c	125614.2+565225	1254+571	1856	± 9	9184	±11	35257	±16	34229	±47	12.17	Q
34o	140700.3+282714	1404+286	872		423	±11	762	±13	1052	±39	11.05	F,4
35d	143645.8+633637	1435+638	16		18		26		79		12.64	F,3
36d	144516.4+095836	1442+101	25		37		76		169		13.63	S,5
37o	150424.9+102939	1502+106	20		30		29		85		11.44	F
38c	161341.0+341247	1611+343	24	± 4	12	± 4	53		141		12.58	F,5
39o	163515.4+380804	1633+382	15		11	± 5	36	± 8	74		12.65	F
40d	163813.4+572023	1637+574	38		39		68		206		12.09	F
41o	164258.8+394836	1641+399	144	±10	338	±11	766	±18	1277	±56	12.91	F,9
42d	183250.1+283335	1830+285	38		44	±15	101		564		12.04	I,5
43d	200324.1-325145	2000-330	19		35		29		85		13.28	F
44d	210138.8+034131	2059+034	23		49	±11	174	±12	114		13.13	F
45c	212912.1-153841	2126-158	44		81		84	±20	192		13.60	F
46o	213135.2-120704	2128-123	44		96		59		185		11.64	F,3
47c	214712.7-753613	2142-758	33		37		61		220		12.43	F
48o	220314.9+314538	2201+315	62	± 6	111	± 7	126	± 9	85		11.49	F
49c	222547.2-045701	2223-052	168	±11	363	±19	951	±16	1747	±51	13.88	F
50o	225357.7+160853	2251+158	41		112	±18	179	±19	564		12.63	F,2
51d	225717.3+074312	2254+074	41		73		155	+20	366		12.05	I,3
52c	230343.5-680737	2300-683	28		32		52		172		11.61	F
53d	232917.7-473019	2326-477	43		56		60		132		12.56	F,8
54c	234636.8+093045	2344+092	19		71	±13	67	± 8	135		11.98	F,2
55o	234802.6-163112	2345-167	37	±15	94		93	±19	158		11.97	F

REMARKS: F – flat spectrum, S – steep spectrum, I – intermediate spectrum; 1-9 are circumstances of observations [8]

One can see from Tables 3 and 4, these 55 IR/ICRF quasars include 42 sources with flat radio spectrum, 4 – with steep, 8 – with intermediate and only one radio quiet quasar. Evidently the radio quiet quasars have not enough luminosity $L_{60}/L_{\odot}$ to be bright sources in infrared.

CONCLUSION

The comparison of the Neugebauer *et al.* [8] list of 179 quasars observed by IRAS satellite in 1983 with the ICRF list of 608 radio sources [7] had been carried out and 55 common extragalactic sources were found. The major part of them (42) has a flat radio spectrum. On the contrary only radio quiet quasars practically can not be bright sources in infrared.

These 55 IR/Radio sources should be included to the first level IR reference catalogue which is compiled in Kyiv.

They permit, firstly, to establish a direct connection between the infrared and ICRS coordinate systems. It can be used, secondly, to improve in future the connection between radio (ISRF) and optical (HIPPARCOS) coordinate systems [4]. We recommend, therefore, the list of 55 IR/Radio sources for VLBI (or VLA) observations as well as for infrared precise positional observations.

We are going to continue this investigation after identification of ICRF sources with their counterparts from DENIS and 2MASS, after these latters will be published [2].

Acknowledgments. This work was supported by the Ukrainian Foundation of the Fundamental Research, Grant 2.4/8.
The discussion of this work with Dr. Chopo Ma was highly appreciated.

REFERENCES

[1] *Beichman C. A., Neugebauer G., Habing H. J., et al.* IRAS Catalogues and Atlases: The Explanatory Supplement / Ed. T. J. Chester.–NASA RP-1190.–1987.–**2–6**.

[2] *Epchtein N.* // Astrophys. and Space Sci. Lib.–1997.–**230**.–P. 3–9.

[3] *Hindsly R., Harrington R.* // Astron. J.–1994.–**107**.–P. 280–286.

[4] *Kharin A. S.* // Proc. 3rd Orlov Conf. / Ed. Ya. Yatskiv.–Kyiv, 1994.–P. 81–84.

[5] *Kharin A. S.* // Systems De Reference Spatio-Temporels / Eds J. Vondrak, N. Capitaine.–Prague, 1997.–P. 126–129.

[6] *Kharin A. S., Molotaj O. A.* // Systems De Reference Spatio-Temporels & IX LOHRMANN-KOLLOQUIUMM / Eds M. Soffel, N. Capitaine.–Dresden, 1999.–P. 55.

[7] *Ma C., et al.* // Astron. J.–1998.–**116**.–P. 516–546.

[8] *Neugebauer G., et al.* // Astrophys. J.–1986.–**308**.–P. 815–828.

[9] WG IERS // IAU Inform. Bull.–January 1995.–N 74.–P. 3–18.

22 GHZ RADIOMETER FOR VLBI STATION "SIMEIZ"

N. S. Nesterov[1], **A. E. Volvach**[1], **I. D. Strepka**[1],
V. M. Shulga[2], **V. I. Lebed'**[3], **A. M. Pylypenko**[3]

[1] *Crimean Astrophysical Observatory, RT-22, Katsively, 98688 Crimea, Ukraine*
e-mail: `volvach@crao.crimea.ua`

[2] *Institute of Radio Astronomy, NAS of Ukraine*
4 Chervonopraporna St., 61002 Kharkiv-2, Ukraine

[3] *Joint-Stock Scientific-Production Enterprise "Saturn", 03148 Kyiv, Ukraine*

The 22 GHz VLBI cooled radiometer was put into operation at 22-m radio telescope of the CrAO (station "Simeiz" of the European VLBI Network). The System Equivalent Flux Density was measured as 2300 Jy in zenith.

VLBI is a very powerful tool for study of the Active Galactic Nuclei (AGN), Star Formation Regions (SFR), and Stars: it gives a possibility to study their structures with angular resolution up to submilliarcsecond, which is not reached in other regions of the electromagnetic spectrum.

The radio telescope of the Crimean Astrophysical Observatory with a 22-m dish (RT-22) has taken part at VLBI observations in 1969 using Mark-I system and rubidium frequency standard. Then the RT-22 was included as an international station "Simeiz" into the global European VLBI network for astrophysical studies. The station was equipped with Mark-II system and hydrogen maser frequency standard with stability to be equal to 10^{-14}. These observations were carried out by CrAO and Institute of Space Research of RAS at 1.35, 2.8, 6, 18, 49 and 92 cm. In June 1994, the RT-22 was equipped with Mark-IIIA terminal supplied by GSFC NASA.

In August 1999, the 22 GHz VLBI cooled radiometer was put into operation at the RT-22. The low noise cryogenically cooled receiver was developed and manufactured by Joint-Stock Scientific Production Enterprise "Saturn" with assistance of the Crimean Astrophysical Observatory and the Institute of Radio Astronomy of NASU. Figure 1 shows the block scheme of the low noise 22 GHz receiver and Table 1 gives the receiver parameters. The cryostat with cooled pHEMT amplifier, the phase and the amplitude calibration units have been installed in the secondary focus of the antenna.

Table 1: The parameters of 22 GHz receiver

Parameter	*Range*
Input frequencies	22.0 – 22.5 GHz
Input noise temperature	45 K
IF output frequencies	100 – 600 MHz
Reference frequency	5 MHz

All measurements of the noise of radiotelescope-radiometer system were made by Mark-IIIA and Field System 8.2. System Equivalent Flux Density (SEFD) was measured by observing radio sources with known flux densities: DR21, Virgo-A, Cygnus-A, Taurus-A. The power pattern of antenna was equal to $170''$. SEFD was measured as 2300 Jy in zenith, this value of SEFD corresponds to the effective area of 180 m^2 and system noise temperature of 150 K.

The installation of the new low noise receiver has to be considered as the first stage of the upgrading of receiver base of "Simeiz" station which will allow to continue astrophysical single dish and VLBI observations with a high sensitivity.

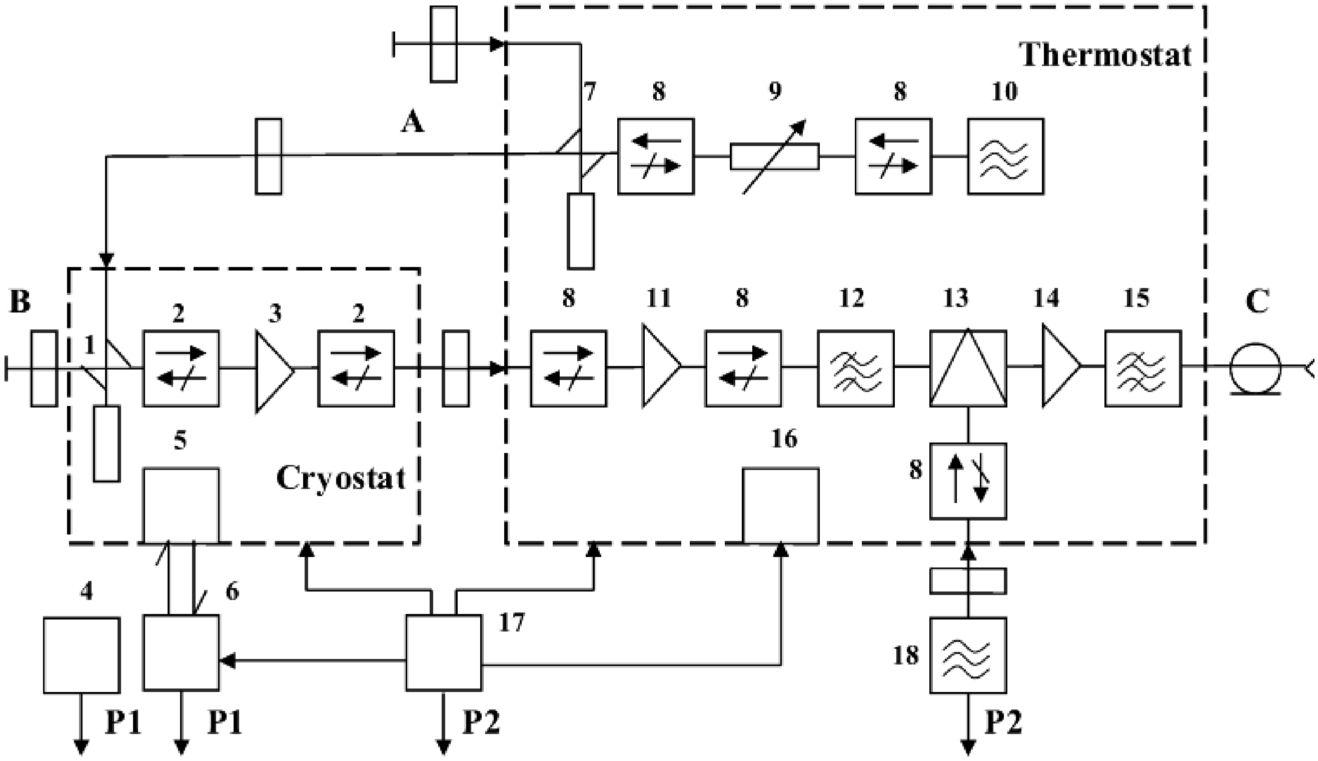

Figure 1: The block scheme of 22 GHz receiver:

1 – directional coupler,
2 – cooled isolator,
3 – cooled amplifier,
4 – vacuum system,
5 – cooled hit,
6 – compressor,
7 – directional coupler,
8 – isolator,
9 – attenuator,
10 – noise generator,
11 – amplifier,
12 – band-pass filter,
13 – balance mixer,
14 – IF amplifier,
15 – band-pass filter,
16 – thermostat system,
17 – power supply and control block,
18 – LO,
A – input phase calibration,
B – input 22.0 – 22.5 GHz,
C – output 100 – 600 MHz,
P1 – power 380 V,
P2 – power 220 V

Session 2. VLBI for Geodynamics

Convener: Prof. Valeri Shulga (IRA NASU, Ukraine)

GEODETIC VLBI EUROPEAN CAMPAIGNS: SCHEDULE, OBSERVATION, CORRELATION, ANALYSIS

M. Sorgente

Geodetic Institute of the University of Bonn (GIUB) Germany
e-mail: sorgente@itis.mt.cnr.it

Nowadays geodetic VLBI is a routine process which runs as a service. Main phases of this conveyer are following: scheduling observations which is done by an Operating Centre, observations which are carried out simultaneously by 2–20 stations for 24 hours, correlation which is done by a dedicated supercomputer called "correlator", post-processing, submission of databases with observations to Data Centres and final analysis. Successful VLBI experiment is possible only as a result of coordinated efforts of many individuals. I will expose how this conveyer is working smoothly. I will consider in details the correlation phase and the specific problems which can be detected during correlation: radio interference, spurious signal in phase calibration, errors in tapes reading and how these factors affect the final results. A Geodetic VLBI European session consists of making a schedule, observing, correlate and analyse the data collected from all the stations. I will do an overview in this report of these points taking more attention of the correlation, the problems that I find during correlation and present status of the Bonn correlator.

INTRODUCTION

A Geodetic VLBI session is carried out simultaneously by 2–20 stations for 24 hours, which observe at the same time a set of radio-sources. The selected sources should be compact sources to have a very strong SNR at X band (about 3.6 cm wavelength) and at S band (about 13.4 cm wavelength) and should not have an appreciable proper motion.

The observations are scheduled with the aim to have an uniform distribution of sources in the sky observed from each station during the observing time.

During the observation each station produces a log file, where all the data about the ongoing observation are stored.

The correlation process consists of three main parts, the fringe search, the correlation and the post-processing.

The correlated data are then ready to be analysed geodetically and/or astronomically.

SCHEDULING AND OBSERVING

The schedule of a VLBI session is performed on the basis of the availability of as many telescopes as possible for that session. Each geodetic sessions takes normally 24 hours.

The most important aspect preparing a schedule for a geodetic observation is that from each telescope the sources have to be observed more or less uniformly in all the azimuth direction and for all the elevations.

In a geodetic observation it is not important that all the stations have to observe the same source at the same time and for the same time period. The SNR for each baseline must be strong enough to obtain good fringes during correlation, for this reason the radiotelescopes that have a good SEFD, can observe the source for smaller amount of time (as minimum 90 sec.), while the smaller telescopes have to observe the sources for longer time.

During the observation each station produces a log file, where all the informations about the ongoing observation are stored. There are informations about the setup of the recorder, the system temperature of the receiver, the configuration of the recorder the parity error rate of the writing system *etc.*

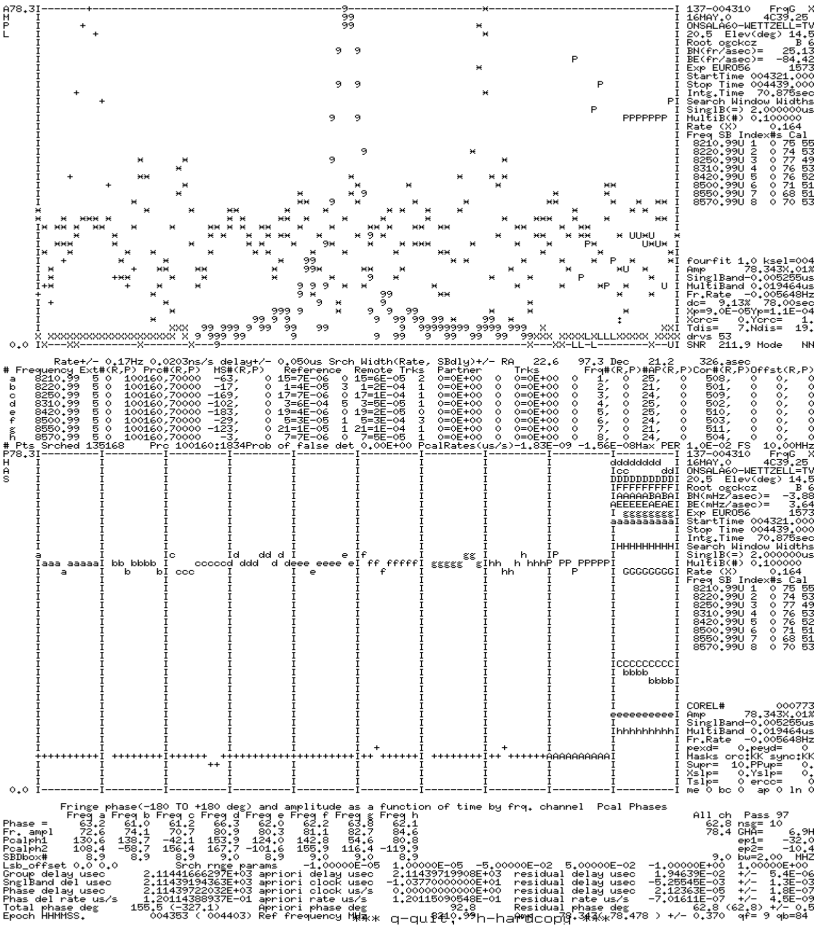

Figure 1: Mark III fringe plot

When the observation ends the operators at the telescope have to put the log files into one data centre (f.e. CDDISA) and to send the recorded magnetic tapes to the correlator centre that is in charge for that experiment.

CORRELATION AND POST-PROCESSING

As soon as all the log files, the schedule file and all the magnetic tapes are collected by a correlator centre the Fringe search of the new experiment starts.

Some steps have to be done before starting the correlation. The first is to give a number to the new experiment, because at a correlator all the experiments have a code name that is only numeric and not alfanumeric.

Then some control files have to be created. The first control file is extracted from the scheduling file and contains informations as the a priori coordinates of the stations, clock offsets and drift between the maser at the stations and the reference time (GPS time), track position for each pass and informations about each scan. The second control file is extracted from the stations log files and it contains informations such as the code of the recorded tapes at each station, beginning and ending time-footage of the scan for each station and on which tracks the data were recorded. The transfer files are the last control that have to be prepared. The files have information about which scans and which baselines have to be correlated.

The correlation process consists of three main parts, the fringe search, the correlation and the post-processing. The fringe search has the purpose to determine the offset between the maser at the stations with an accuracy better than 0.05 μsec, to check the quality of the data and some other parameters as the right footage and head position and which is the best combination recorder-tape for all the stations.

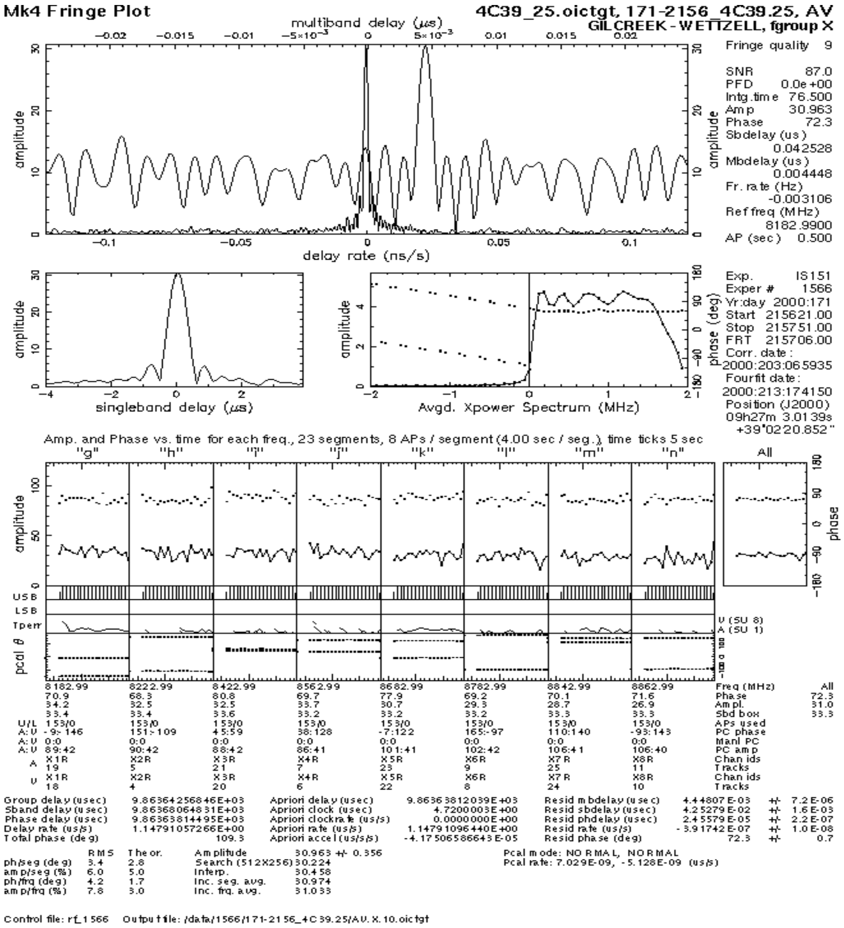

Figure 2: Mark IV fringe plot

When everything is prepared the correlation can start. The raw correlated data are transparent for the operators at the correlator, for this reason is started in an automatic way a post-processing software. The output of this software can be seen on the screen as fringe plots. Two examples of fringe plots, one from Mark III and one from Mark IV correlator, are shown in Fig. 1 and Fig. 2, respectively.

The most important informations that can be extracted from a fringe plots are: the baseline, the source, the elevation of the source over the two station, the single band delay, the multi band delay, the SNR, information about the phase calibrator, the fringe amplitude and the residual fringe phase for each observed channel. The quality of data correlated for each baseline and each scan are then classified with a quality factor (q. f.) code. It ranges from the values 9 to a value 0. The value 9 is given when all the parameters are good, then the values decrease if the residual fringe phase, or the fringe amplitude for each are spread inside a single channel or they have different average values. The worse case is qualified with a q. f. 3. If the fringe amplitude is at one channel more than 50% lower than the average value the q. f. assigned at that scan is 2. A signal amplitude of the phase calibrator lower than the minimum acceptable threshold classifies the scan with a q. f. 1. An SNR lower than 7 is qualified with a q. f. 0 and means that the data are not recoverable. Other q. f. code can be assigned as q. f. "D" if the parity error rate with whom the data are written on the tape is to high, so all data of one or more channels are not recoverable. The q. f. "E" is given if the peak of the multiband delay is not central peaked, but it is very close at the border of the window.

PROBLEMS AND SOLUTIONS

The most common problems that can be detected at the correlator are:

a) the clock offset between the formatter and the GPS time is not correct. This is usually solved by getting only one frequency and looking if the true clock offset is in a larger window of about 50 μsec;

b) the data recorded on one tape have a high number of parity error rate that does not allow to recover at all the data on one or more tracks. The parity error threshold can be erased for the station whose data are bad. It can be done checking that the signal's quality does not decrease too much;

c) one or more frequencies are not at all recoverable at one station or for one baseline. Then all data of this station, or of this baseline are refringed discarding these frequencies;

d) also if the fringe amplitude is at one channel more than 50% lower than the average value at more than 30% of the scans this frequency is discarded in the final fringe;

e) an amplitude too low for the phase calibrator signal at one station can be eliminated using the manual phase calibration. It consists of getting one scan with a strong SNR and giving at each channel the values that allows to adjust the residual fringe phase for all the channels in the selected scan and to apply that values for all data of the station.

When the correlation and the post-correlation processes are ended and all these problems are solved, the data can be analysed with the geodetic CALC/Solve software.

CONCLUSION

Most of the problems that can happen during the observation can be recovered in some way in the correlation and the post-correlation process. Nevertheless, some of the consequences will come out only later during the analysis. For example we see bigger error in the least squares fitting of the baseline lengths.

THE APPLICATIONS OF VLBI IN GEODESY AND GEODYNAMICS

C. Ma

NASA Goddard Space Flight Center, Code 926
Greenbelt, Maryland, 20771, USA
e-mail: cma@virgo.gsfc.nasa.gov

The applications of VLBI in geodesy and geodynamics arise from its ability to construct a terrestrial reference frame and a celestial reference frame from geometrical measurements and to determine the relationship between these frames without recourse to other information. VLBI contributes directly to the ITRF, defines the ICRF and provides stable, consistent EOP time series with decadal to subdiurnal resolution. The results derived from VLBI include refinement of plate tectonic and deformation zone models and detection of variations in geophysical fluid motions.

INTRODUCTION

VLBI is a geometrical technique that measures the difference in time of arrival of a wave front at two widely separated antennas with precision of 10–15 picoseconds. The radio emitters observed for geodesy are extragalactic objects, generally quasars, so the wave fronts are planar. A 24-hour geodetic session may observe up to 80 radio sources around the entire sky and include up to 20 stations worldwide. The limitation on the number of sources is related to the sensitivity and slewing speed of the antennas available for VLBI geodesy while the limit on stations in a single observing network is imposed by the size of existing VLBI correlators. Using the set of time differences (delays) from a session the relative positions of the sources and of the stations can be estimated with high precision and accuracy, taking into account such effects as relativity, orbital and diurnal velocity, ground motions from solid Earth and ocean tides, propagation medium delays including tropospheric gradients, atmospheric loading, and station clock behavior. The data from the entire span of dual-frequency geodetic VLBI observations can be analyzed uniformly and concatenated to derive station velocities or time series of station positions and baseline components. While the celestial reference frame of extragalactic radio sources is conceptually fixed in a kinematic sense, in actuality there is some amount of noise and pseudosystematic behavior in the source positions because of changes in source structure. The limit of accuracy of individual source positions is estimated to be 0.25 milliarcsecounds [1], so the celestial reference frame is not the limiting factor for current VLBI applications in geodesy and geodynamics. The reference frame of extragalactic objects measure by VLBI was adopted by the IAU as the ICRF (International Celestial Reference Frame) effective 1 January 1998.

GEODYNAMICAL RESULTS FROM VLBI

The measurements of station positions from VLBI are intrinsically relative to each other since the VLBI delay observable is derived from a baseline connecting two stations. Likewise relative velocities can be derived from the two decades of VLBI data, but for geodynamical interpretation individual station velocities are useful. By suitable no-net-translation and no-net-rotation conditions relative to an *a priori* velocity model, the set of relative velocities can be separated into individual station velocities. In practice the velocity frame of NUVEL-1A NNR is conventionally used with the conditions applied to stations whose relative velocities agree with NUVEL-1A. It should be noted that no vertical velocity condition need be applied, but the applicability of such no-net-translation/rotation conditions requires a global distribution of the specified stations. Figure 1 shows the velocities of selected VLBI stations in the NUVEL-1A reference frame. Since NUVEL-1A NNR is defined geometrically rather than geophysically, all stations show motion arising from their respective plate motion. Figure 2 shows the difference between the VLBI horizontal velocities and the underlying plate velocities. The stations without vectors in Europe, North America and Australia show that these parts of the plates are essentially rigid. In contrast the large vector on the west coast of South America indicates substantial deformation caused by the subduction of the Nazca plate. The differing vector magnitudes and directions in western North America show a more complex pattern: slight deformation in the interior, marked deformation nearer the coast where the North American and Pacific plates interact, a small discrepancy at the coast (this point is modeled as being on the Pacific plate), and a northward deformation near the U.S.-Canada border.

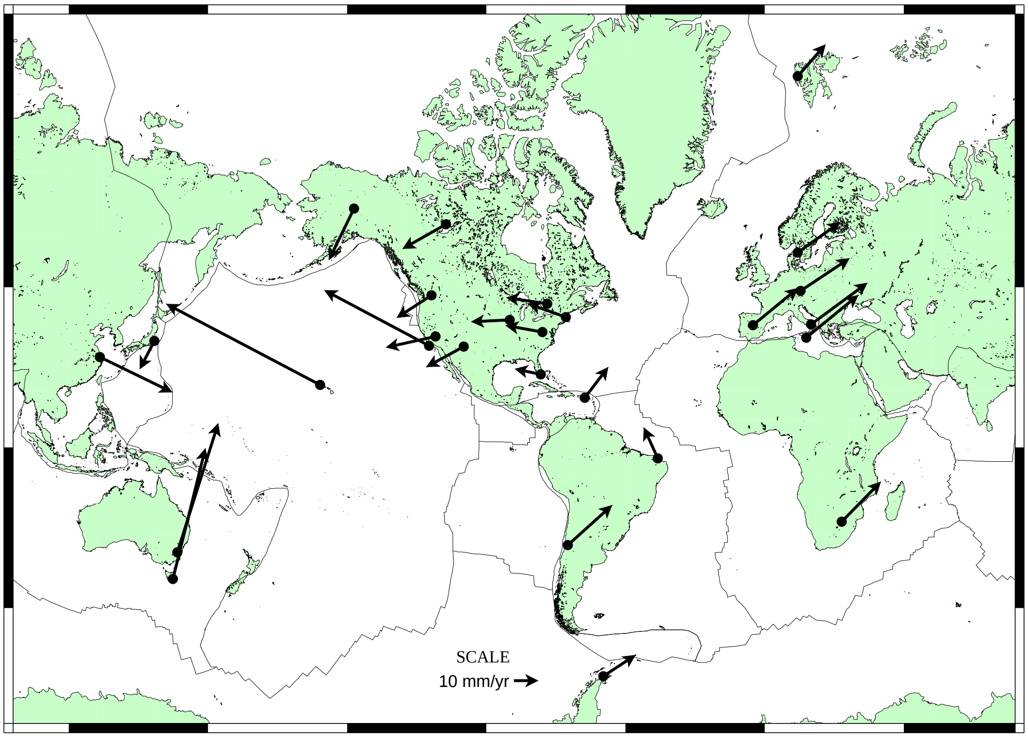

Figure 1: Selected VLBI velocities in the NUVEL-1A NNR reference frame

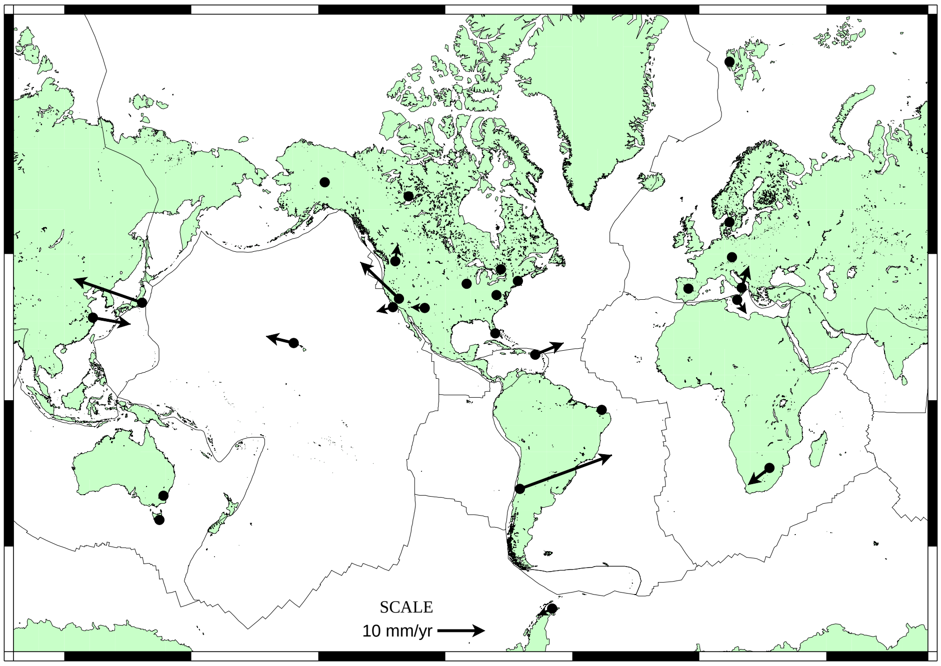

Figure 2: Differences between VLBI velocities and their corresponding plate models. The reference frame is NUVEL-1A NNR. Velocity residuals less than 2 mm/yr are not displayed

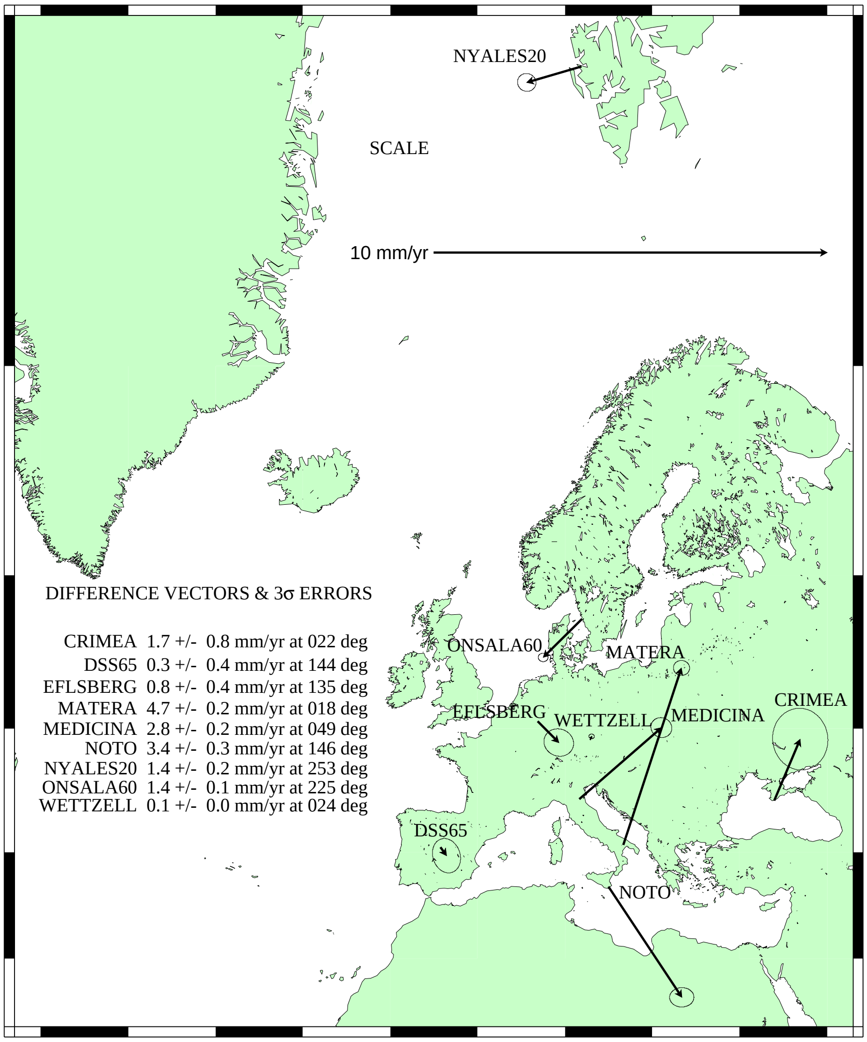

Figure 3: Horizontal velocity adjustments at selected European sites. Differences are from the rigid plate model. The reference frame is NUVEL-1A NNR. Error ellipses are 3σ

The vector in Japan shows the deformation caused by the Pacific plate while the vector on the coast of China is a result of the Indian-Eurasian collision. The vector in the middle of the Pacific probably indicates an overall error in the NUVEL-1A model rather than a midplate deformation, but the vector in South Africa is indicative of intraplate rifting.

Figure 3 shows more details of horizontal motions in Europe. It can be seen that Spain, Germany, Sweden and Spitsbergen are relatively rigid. In Italy the interaction of the Eurasian and African plates causes larger, significant deformations. The station Noto is modeled as being on the African plate. It should be noted that the error related to the reference frame definition, *i.e.*, the choice of stations in the no-net-translation/rotation conditions, is estimated to be 0.4 mm/yr and must be kept in mind in interpreting the velocity of an single station in isolation.

Figure 4 illustrates the ability of VLBI to measure vertical motions. Vertical motions are inherently more difficult than horizontal because of asymmetry; antennas do not point into the ground. In addition, an elevation cutoff around 7 degrees is usually imposed in analysis because of difficulties in properly modeling the troposphere at lower elevations. Formal errors of vertical rates are generally two to three times greater than the corresponding horizontal errors. Nonetheless it can be seen that significant vertical rates are found at Onsala (from post-glacial rebound), at Medicina (probably from ground water withdrawal) and at Ny Alesund (of as yet unknown cause for such a high value).

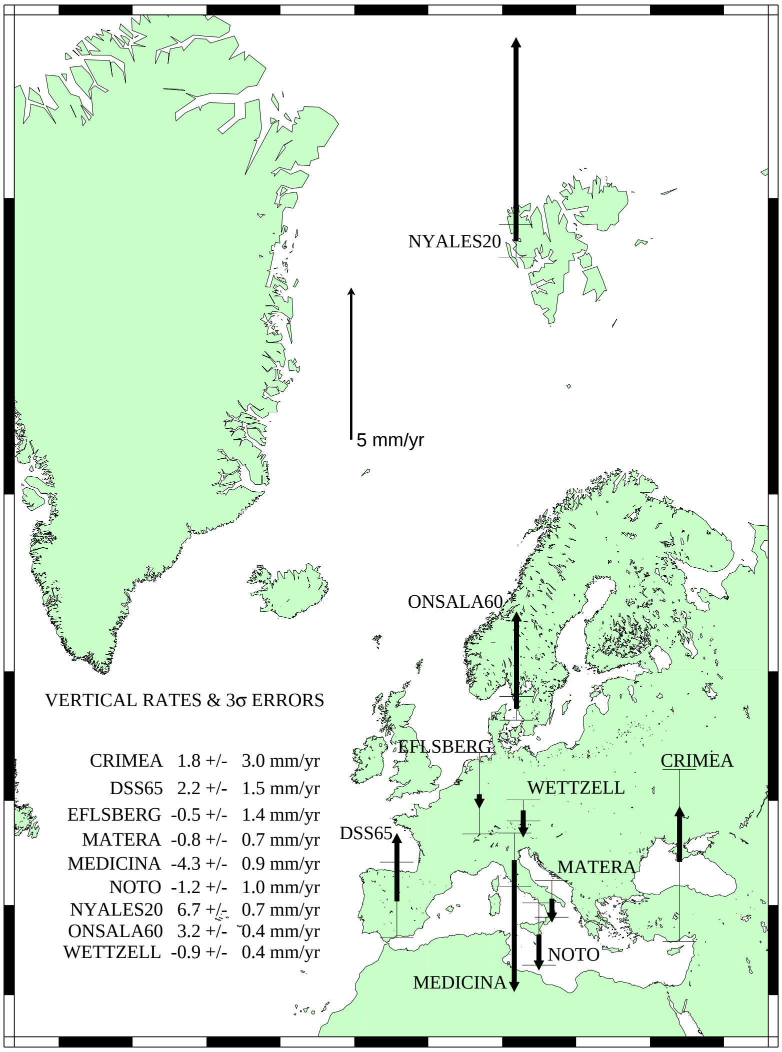

Figure 4: Vertical velocity adjustments at selected European sites. Error bars are 3σ

VLBI AND THE ITRF (INTERNATIONAL TERRESTRIAL REFERENCE FRAME)

Results from VLBI analysis are essential and significant inputs to the definition of the International Terrestrial Reference Frame. Although VLBI has no tie to the geocenter, it provides a self-consistent set of station positions and velocities that can be attached to a geocentric origin by suitable conditions. VLBI analysis centers have contributed regularly to the various realizations of the ITRF. For ITRF2000 three such submissions including 130 stations were used in the combination. The scale of the VLBI terrestrial reference frame depends on the accuracy and completeness of the theoretical delay model and the troposphere model. With recent improvements such as the consensus model in the 1996 IERS Conventions [2], the Niell mapping functions [3], and estimates of tropospheric gradients including *a priori* mean north-south values, the VLBI scale should be accurate at the 1 ppb level. Both VLBI and SLR values were used in defining the scale of ITRF2000.

The two-decade span of VLBI observations provides a long interval for accurate determination of station velocities. Figure 5 shows the precision of VLBI velocities. In general, the triangles (horizontal velocity formal errors less than 0.5 mm/yr) also correspond to currently active stations. The cluster of less precise velocities in Alaska and western U.S. are from measurement with mobile VLBI systems in the 1980s and early 1990s. When projected to the reference epoch of ITRF2000, these mobile positions as well as positions from other now inactive stations like Florida and Chile, have large errors, but some are still useful as collocations between different space geodetic techniques and ties between their respective reference frames.

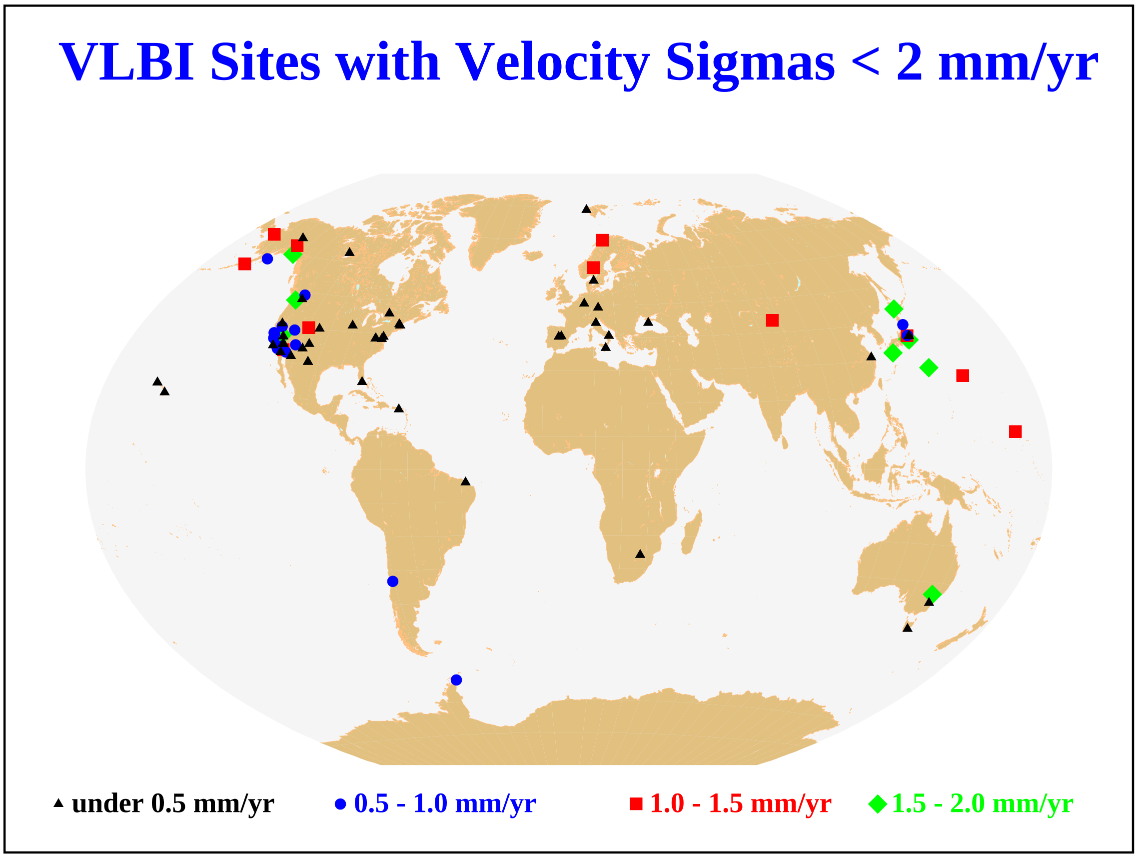

Figure 5: VLBI sites with horizontal velocity sigmas less than 2 mm/yr

VLBI AND EARTH ORIENTATION PARAMETERS

Of the space geodetic techniques only VLBI has direct access to the celestial reference frame. Consequently, any information about long term UT1 and nutation/precession, three of the five Earth orientation parameters, must come from VLBI measurements. Analysis of satellite data like SLR or GPS relies on UT1 from VLBI to align their celestial reference frames, which are the orbital planes. However, because of practical limitations in station availability and correlator capacity VLBI EOP measurements cannot be done continuously, unlike satellite measurements. At present there are between two and three 24-hour sessions per week on average, and increased observing is planned for the future. In addition, there are nearly daily, 2-hour, one-baseline observations for UT1 with reduced precision. Even with uneven temporal resolution VLBI EOP times series have been used to measure variations in atmospheric angular momentum related to seasonal weather and larger disturbances like El Nino/La Nina. The diurnal and semidiurnal bands in UT1, derived from spectral analysis of hourly VLBI time series or by direct estimation of harmonic coefficients, show the effects of ocean tides. The time series of deviations in longitude and obliquity from the 1980 IAU nutation/precision model provided information on the shape and coupling of the core-mantle boundary as well as constraints for the new nutation model adopted by the IAU in 2000.

REFERENCES

[1] *Ma C., et al.* The International Celestial Reference Frame as Realized by Very Long Baseline Interferometry // Astron. J.–1998.–**116**.–P. 516–546.

[2] *McCarthy D.* ed. IERS Conventions (1996) // IERS Tech. Note 21.–1996.–Paris Obs.–Paris.

[3] *Niell A.* Global Mapping Functions for the Atmosphere Delay at Radio Wavelengths // J. Geophys. Res.–1996.–**101**.–P. 3227–3246.

PERFORMANCES OF CRIMEA'S RADIOTELESCOPE IN THE GEODETIC VLBI EUROPEAN CAMPAIGNS

M. Sorgente

Geodetic Institute of the University of Bonn (GIUB) Germany
e-mail: `sorgente@itis.mt.cnr.it`

The Crimea station could not take part at all the scheduled Geodetic VLBI European sessions due to technical problems. It was a pity because the quality of the results obtained was good when it could participate. Still some problems remain to be solved. In this report I will show the main problems that were detected during the correlation and the analysis. At mainly these problems concern the system temperature and the voltage of phase calibration signal.

INTRODUCTION

The Crimea station is the only eastern station that takes part at the European Geodetic VLBI network and this explains the importance of this station in the network. For this reason it was accepted as an external member inside the European Geodetic VLBI Project and it was scheduled as many times as possible.

The Crimea station could take part successfully since December'98 at only 3 sessions:

Euro46: 98 December 14

Euro51: 99 October 11

Euro52: 99 December 13

The station was scheduled in 8 other sessions. However, mostly due to unforeseen power cuts, the observations could not be carried out. Of course it is hoped that this situation will improve in the future. During one session the operator had to shut down the system due to failure of electricity power and to reboot the system, it happened during Euro52 session. This lack of electricity introduced a clock jump of about 0.5 μsec. The operator had to stop the observation of Euro55 session one hour after the beginning due to lack of power and he could not restart to observe. The Euro46 session started five hours later because the telescope was not moving properly.

The system temperature and the low voltage of phase calibration signal problems are perhaps also closely related to an inadequate electricity power at the station.

PROBLEMS AT CRIMEA STATION AS SEEN FROM THE CORRELATOR

The cooling system seems to be at the heart of the problems with system temperature at Crimea station. In Table 1 it is possible to see the mean values of the system temperature in the zenith direction of Euro46, Euro51 and Euro52 session.

Table 1: Mean value zenith system temperature at Crimea

Channel	Euro46	Euro51	Euro52
BBC # 1 (8210.99 MHz)	64.6	60.4	333.2
BBC # 2 (8220.99 MHz)	65.9	62.4	313.3
BBC # 3 (8250.99 MHz)	73.0	78.3	373.5
BBC # 4 (8310.99 MHz)	75.2	69.0	416.0
BBC # 5 (8420.99 MHz)	48.1	37.1	
BBC # 7 (8550.99 MHz)	52.3	41.0	272.8
BBC # 8 (8570.99 MHz)	47.9	39.5	262.5
BBC # 9 (2212.99 MHz)	89.6	341.2	458.5
BBC # 10 (2227.99 MHz)	87.8	289.5	400.3
BBC # 11 (2237.99 MHz)	85.8	262.9	401.5
BBC # 12 (2267.99 MHz)	89.7		
BBC # 13 (2287.99 MHz)	90.2	236.0	523.1
BBC # 14 (2292.99 MHz)	88.4	246.9	491.8

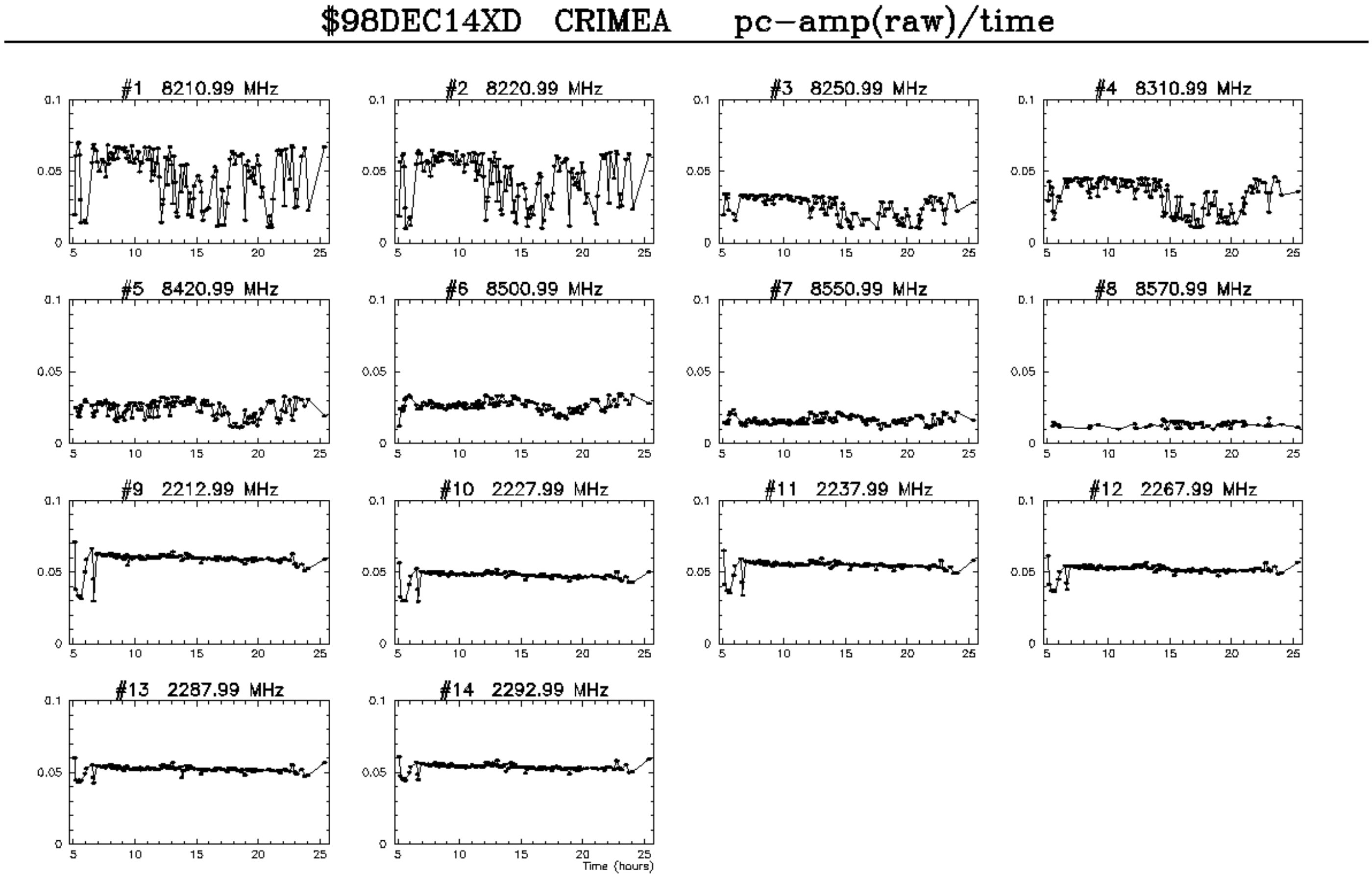

Figure 1: Raw phase calibration amplitude versus time in Euro46

In Euro52 session the value of the system temperature were unrealistically high at all channels (see Table 1). The average system temperature was over 320K at X band and over 450K at S band.

In Euro51 session instead the system temperature had acceptable values of about 55K at X band (see Table 1), but at S band was over 270K.

Acceptable system temperature values are for Crimea station about 60K at X band and about 80K at S band, as the values we had in the Euro46 session.

The values reported for the BBC 6 were at each session in overflow, also when other channels at X band had acceptable values. It is due to a technical problem of this channel, because this BBC is not in the same box as the others and feels the influences of room temperature; for this reason it was discarded from Table 1.

The phase calibration signal is generally low, also if not always lower than the minimum acceptable threshold (see Fig. 1).

The windows for an acceptable phase calibration signal is between 0.01 and 0.1 part of the total signal, but it would be better if the signal is higher than 0.05. As we can see in Fig. 1 only at S band the raw phase calibration signal was good. The phase calibration signal was weak or too much spread at X band, also if the system temperature was normal (Table 1).

Manual phase calibration had to be applied at all these experiments.

At the Euro52 session the data at Channel #5 and #7 (frequencies 8420.99 and 8550.99 MHz) were not always recoverable, for this reason they have been discarded in the final fringe.

CONCLUSION

Crimea station is a very important for the European Geodetic VLBI network. Unfortunately, it has not yet a good reliability due to technical problems.

It would be mighty desirable if the efforts to improve the performance of the Crimea Station, in view of the so important position inside the tectonic plate, which cannot be substituted by other radiotelescopes.

SIMEIZ RADIO TELESCOPE: IVS NETWORK STATION, SINGLE DISH S/X BAND OBSERVATIONS

A. Volvach[1], **N. Nesterov**[1], **L. Petrov**[2]

[1] *Crimean Astrophysical Observatory, RT-22, Katsiveli, Crimea, 98688 Ukraine*
e-mail: volvach@crao.crimea.ua
[2] *Code 926, NVI, Inc./NASA Goddard Space Flight Center, Greenbelt, MD 20771 USA*

1. INTRODUCTION

The Laboratory of Radioastronomy of the Crimean Astrophysical Observatory (CrAO) operates with 22-m radio telescope (RT-22) located on the Black Sea coast of the Crimean peninsula in 60 meters from sea. Table 1 shows the RT-22 antenna parameters.

Table 1: The RT-22 antenna parameters

Diameter D, m	22
Surface tolerance, mm (root mean square)	0.25
Wavelength limit, mm	2
Feed System	Cassegrain system or primary focus
Focal length F, m	9.525
Focal ratio F/D	0.43
Effective focal length for Cassegrain system, m	134.5
Mounting	Azimuth-Elevation
Pointing accuracy, arc sec.	10
Maximum slewing rate, degree/sec	1.5
Maximum tracking rate, arcsec/sec	150
Working range: in azimuth, degrees (0 to South)	–270 – +270
in elevation, degrees	0 – 85

The RT-22 operation is supported by control system, consisting of two encoders with accuracy of about 3 arcsec (rms), personal computer, CAMAC, quartz time standard, electric engines and other needed equipment and software. The fast RT-22 movement is supported by 2 engines each with 20 kW power, which are used for rapid change of pointing or for movement of the RT-22 from one source to another. 2 kW engines are used for tracking of sources.

The telescope was constructed in 1966 and the VLBI Simeiz station at the RT-22 started operation in cooperation with some American stations in 1969 using Mark-I system and rubidium standard (Broderick *et al.*, 1970).

Later the RT-22 was included into the global VLBI network for study of astrophysical objects. The Simeiz station was equipped with Mark-II system and hydrogen maser frequency standard with stability 10^{-14}. The CrAO and the Institute of Space Research carried out the observations at 1.35, 2.8, 6, 18, 49 and 92 cm wavelengths.

In June 1994 the Simeiz station was equipped with Mark-IIIA terminal provided by NASA GSFC and low noise receivers of S/X bands supplied by the Institute of Applied Astronomy (Clark *et al.*, 1995).

Since this time the RT-22 was included into international geodetic VLBI network under the "Crimea" name. Low noise cooled receivers of S/X bands with dual frequency feed have been installed in the prime focus of the antenna. Dual feed is capable to receive both LCP and RCP. The feed is connected to receivers by straight waveguide in X band and by the short coaxial cable in S band.

S and X band receivers have been constructed for superheterodin scheme with FET amplifiers. Fronted directional coupler and FET amplifiers are cooled by microcryogenical system to obtain low noise temperatures. Table 2 shows the parameters of radio telescope – radiometer system.

Focusing both for S band and for X band (more precisely) was made. The power pattern of antenna has been measured using the radio sources: Taurus-A, Virgo-A, Cas-A and Cygnus-A. System equivalent flux densities (SEFD) was measured using radio sources with known flux density. The increasing of Tsys for angles lower then

Table 2: The radio telescope – radiometer parameters

Band	Input frequencies	LO	Tsys	System equivalent flux density
S	2.15–2.5 GHz	2.02 GHz	75 K	1100 Jy
X	8.18–8.68 GHz	8.08 GHz	50 K	780 Jy

30 degrees is caused by rise of atmosphere optical depth. Characteristics obtained correspond to the standards of VLBI low noise system.

Geodynamical VLBI observations are conducted in 24 hours sessions scheduled 6-15 times per year. Observational programs are a part of common efforts for maintenance of terrestrial reference frame, celestial reference frame and monitoring Earth orientation parameters carried out by international community under the auspices of International VLBI Service (IVS) (Vandenberg, 1999). Data are recorded on magnetic tapes, which are shipped to correlator centers for further correlation and fringing. Fringed data are freely available via Internet for scientific analysis for everybody after 1–2 months after observations.

2. OBSERVATIONS AND DATA ANALYSIS

2.1 IVS

All available dual-band geodetic MARK-III VLBI observations for 20 years: 1979.59–1999.82, 2 931 sessions, 2 708 795 observations including 34 successful sessions with participation of the Simeiz station for 4.5 years: 1994.48–1998.96 with 17 655 good measurements of group delays were used in an analysis.

The Simeiz station moves with respect to the Eurasian tectonic plate considered as a rigid with rate 2.1 ± 0.9 mm/yr in a north-east direction. Thorough investigation of possible systematic effects has been done and the reliability of the estimate of the uncertainty has been evaluated. Performance of the receivers and H-maser were examined. The stability of the station with respect to local marks was investigated and an inclination of the azimuthal axis (Pisa effect) of the telescope with velocity $2''\!.6$ per year was disclosed.

We obtained the following position of the Simeiz station at the epoch 1997.0 and its rate of change in the ITRF97 system:

$$
\begin{array}{ll}
X = 3785231.073 \pm 0.004 \ \text{m} & \dot{X} = 5.5^{-10} \pm 0.2^{-10} \ \text{m/sec} \\
Y = 2551207.417 \pm 0.003 \ \text{m} & \dot{Y} = 4.9^{-10} \pm 0.1^{-10} \ \text{m/sec} \\
Z = 4439796.362 \pm 0.006 \ \text{m} & \dot{Z} = 2.3^{-10} \pm 0.2^{-10} \ \text{m/sec}
\end{array}
$$

The details of the scientific analysis are given in Petrov *et al.*, 2000.

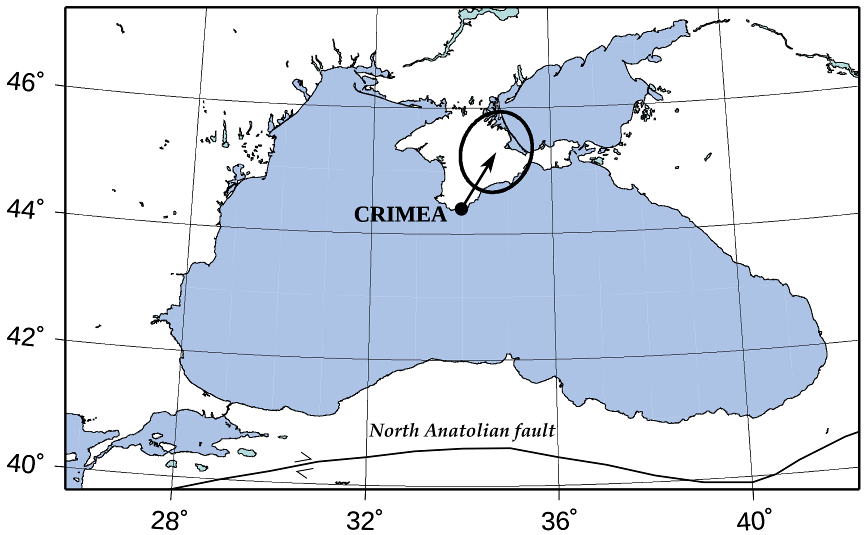

Figure 1: Motion of the station Simeiz

2.2 SINGLE DISH

The antenna temperatures from sources were measured by the standard ON–OFF method. Before measuring the intensity, we determined source position by scanning. The radio telescope was then pointed alternately at source and at the distance of 5 beamwidths off source. The antenna temperature from a source was defined as a difference between radiometer responses averaged over 10 s at two different antenna positions. Depending on the intensity of emission from sources, we made a series of 20–60 measurements and then calculated the mean signal intensity and estimated the rms error of the mean. The fluxes from the objects under study were calibrated using measurements of the calibration sources Cyg-A, Cas-A, Tau-A, Vir-A, whose flux densities or brightness temperatures are given in Mark-IV Field System Documentation (1993). Converting antenna temperatures to flux densities, we took into account the dependence of effective antenna area A_{eff} on elevation.

Table 3 shows measured flux densities of source at 8 GHz in which Column (1) is IAU source designation; Column (2) and Column (3) is date and time observations, respectively; Column (4) is flux densities; Column (5) is the rms errors of the measured flux densities.

Table 3: Single dish 8 GHz measured flux densities

SOURCE	DAT(YY.MM)	TM(DD.UT)	FLUX(Jy)	SIGM(Jy)
0316+413	97.09	4.931	22.4	1.1
	97.12	10.668	20.9	1.4
0528+134	97.09	5.149	3.3	0.7
	98.02	1.685	3.1	0.9
0552+398	97.09	4.999	5.2	0.5
0642+449	97.09	30.294	1.9	0.3
	98.02	1.622	3.3	0.9
	98.04	20.303	2.7	0.8
	98.06	23.458	1.8	0.4
	98.06	23.478	2.7	0.7
	98.06	23.487	3.0	0.5
1226+023	97.08	29.651	30.5	3.7
1253-055	97.08	29.668	22.3	1.4
2037+421	97.09	4.898	19.2	1.6
	97.12	10.661	21.2	0.7
	98.02	2.344	20.9	1.0
2145+067	98.02	2.355	6.2	1.3
2200+420	98.02	3.406	3.8	1.3
2251+158	98.02	3.417	11.2	1.7

3. DISCUSSION OF RESULTS AND CONCLUSIONS

The 4.5 years of geodetic VLBI observations at the CRIMEA station allow to conclude that the Simeiz station moves with respect to the Eurasian tectonic plate considered as a rigid with rate 2.1 ± 0.9 mm/yr in a north-east direction.

The results of single dish S/X observations of sources used for geodesy investigations can be then reviewed after experiment to check the consistency of data from each source.

REFERENCES

[1] *Broderick J. J., Vitkevich V. V., Jauncey D. L., et al.* // Sov. Astron.–1970.–**47**.–P. 627. (in Russian).

[2] *Clark T. A., Bosworth J., Vandenberg N., et al.* // Astron. Lett.–1995.–**21**.–P. 116.

[3] *Petrov L., Volvach O., Nesterov N.* // Astron. Lett.–2000.–submitted.

[4] International VLBI Service for Geodesy and Astrometry: Annual report / Ed. N. Vandenberg.–Greenbelt, USA, 1999.–P. 308. (Web: *http://ivscc.gsfc.nasa.gov/publications/ar1999/*)

[5] Mark IV Field System, Version 8.2, September 1, 1993.–Space Geodesy Program.–NASA/Goddard Space Flight Center.

VLBI ANALYSIS CENTER AT THE MAO OF THE NAS OF UKRAINE

S. Bolotin

Main Astronomical Observatory, NAS of Ukraine
27 Akademika Zabolotnoho St., 03680 Kyiv, Ukraine
e-mail: `bolotin@mao.kiev.ua`

The current state and activities of the VLBI Data Analysis Center at the Main Astronomical Observatory, Kyiv is described. The new generation of the VLBI data analyzing "SteelBreeze" software is announced.

INTRODUCTION

The VLBI Data Analysis Center at the Main Astronomical Observatory (AC MAO) was established in 1995. The primary goal of the AC MAO is the software developing and the data analysing of the VLBI observations for IERS and IVS submissions. The VLBI data processing has a more than 10 years history at the Main Astronomical Observatory:

- 1990: "KIEV-GEODYNAMICS-R" software was developed by Kur'yanova, Medvedsky and Yatskiv [7]. It was capable to estimate the Earth Orientation Parameters (EOP), coordinates of stations and radio sources by processing series of selected VLBI experiments; the calculations were being conducted on OS 360/370 type computer.
- 1992: Development of the *SteelBreeze ver.*1 software was initiated. This software was fully independent from previous one. Originally, it was created for MS DOS operating system, and then was migrated to Windows 3.1. The software was written on Pascal programming language.
- 1994: Direct estimation of the diurnal and semidiurnal polar motion was made from the CONT'94 VLBI observations (see [2]). The polar coordinates (dX_p and dY_p) and $d(UT1-UTC)$ have been estimated on the 14-days interval with about 5 min resolution.
- 1995: First submission of the "GAOUA R" solution to IERS was made. RSC, SSC and EOP estimations based on 177707 group delays were obtained in this solution.
- 1998: Start of development of the *SteelBreeze ver.*2 software. The new version of the software reflects major changes in technique of developing (*e.g.*, *SteelBreeze ver.*2 written on the $C++$ language, running on Linux, Solaris, FreeBSD and other operating systems, uses Qt widget library for graphics user interface).
- 1999: AC MAO has started to act as the IVS Analysis Center.
- 2000: The source tree of the *SteelBreeze ver.*2 software was realized for public access under the GNU public license.

HARDWARE EQUIPMENT

Data analysis and software developing are executing on an Intel Pentium II 400MHz based computer with 192M RAM. It has a SCSI interface connected to 3 hard disk drives with 9, 4 and 6 Gb capacity (it is allowable up to 15 units). The Main Astronomical Observatory has a 33.6 Kb Internet connection. The computer of the AC MAO is operated by the Linux/GNU system. Despite of so humble hardware equipment, it is possible to make data processing of almost all available VLBI observations. The main limitation in hardware is a narrow bandwidth of an Internet connection, which makes impossible for the MAO to act as an Operation Center of IVS.

STEELBREEZE VER.1 SOFTWARE

SteelBreeze software was developed as a tool for geodetic VLBI data analysis. It uses Least Square estimation of various geodynamical parameters with the Square Root Information Filter (SRIF) algorithm [1]. The SRIF uses the Householder's transformation for matrix triangularization which makes it smart and insensitive for computer roundoff. The SRIF makes also possible to introduce a stochastic model for parameter estimation. *SteelBreeze* was written originally on Pascal programming language with Object Oriented Design.

The software imports the geodetic VLBI observations in different formats (NGS cards, MarkIII databases, VDB binaries). It stores the observations in its own inner binary format as well as catalogues of radio sources, stations of observations, EOP, ephemerides, and some other data sets.

It analyses the VLBI data (time delay) of single and multiple set of sessions. The time delay is modeled according to the IERS Conventions 1996, plus additional models (tectonic plate motions, nutation, wet and hydrostatic zenith delay, mapping function, *etc*). The software makes estimations of the following parameters: Earth orientation parameters, coordinates and velocities of selected set of stations, coordinates of selected set of radio sources, Love numbers, clock function and wet zenith delay.

SRIF algorithm allows to make estimations of unbiased parameters as well as stochastic ones. In the software each estimated parameter can be considered as following:

- global parameter: unbiased estimation of this parameter for all set of selected sessions (typically useful for source and station coordinates estimating, *etc.*);
- local parameter: unbiased estimation of this parameter at each session, the estimates of different sessions are considered to be independent (*e.g.*, EOP);
- local parameter with time propagation: unbiased estimation of this parameter at each session, the estimates of adjacend sessions are dependent according to a given rule;
- stochastic parameter: a behavior of estimated parameter is assumed varying from time to time with a given rule (it is implemented random walk process in the software), this type is useful for estimating of clock parameters and wet zenith delays;
- stochastic parameter with time propagation: the same as above, but adjacend estimations for different sessions are tied with the same rule.

As an example of VLBI data processing using *SteelBreeze* software we present the GAOUA 2000 R 01 solution. The group delay data were acquired on different VLBI networks since January 6, 1998 till December 28, 1999. In total 288583 dual frequency Mark III group delays from 176 sessions were processed.

The initial values of station coordinates were taken from ITRF94. The initial values of station velocities were modeled according to plate tectonic motion NNR-NUVEL1A model. The origin of the obtained realization of terrestrial reference frame was linked to ITRF94 by requiring that the vector sum of the adjusted station coordinates be equal to the corresponding sum for a set of 15 stations. The solution SSC(GAOUA) 00 R 01 consists of the set of coordinates for 26 stations.

The initial values of the radio sources coordinates were taken from RSC(WGRF) 95 R 01 solution. The right ascension origin of the obtained realization of celestial reference frame was defined by setting the sum of right ascensions of adjusted sources equal to the corresponding sum of the sources from RSC(WGRF) 95 R 01 solution for a set of 60 radio sources. The RSC(GAOUA) 00 R 01 solution consists of the set of coordinates of 191 radio sources.

The IAU 1980 Nutation model and initial values of EOP(IERS) 97 C 04 were applied. The polar motion and UT1 were corrected for diurnal and semidiurnal tidal variations according to Herring and Dong [4].

The orientation between terrestrial and celestial reference frames was defined by EOP from EOP(IERS) 97 C 04 solution for the reference date December 28, 1999.

Tropospheric refraction in the local zenith direction caused by hydrostatic and water vapor components of the neutral atmosphere was modeled according to Saastamoinen [6]. The zenith delays have been mapped to line of sight elevations with the MTT mapping function of Herring [3] for both hydrostatic and wet components.

Calibration data collected at each observing site were applied to correct for variations in the electrical lengths of the cables between the radio receivers and the data acquisition systems.

The wet zenith delay and clock offset were estimated as stochastic processes and were modeled as random walk with following magnitudes of power spectral density of ruled white noise: for clock offset 20^2 ps^2/hour, and for wet component of tropospheric delay 1.0 cm^2/hour.

The weighted rms post-fit residuals of this solution was 38.4 ps.

The second example of data processing is focused on estimating the polar coordinates and the Earth rotation with a high time resolution. For this purpose we processed the observations of the NASA-R&D network during the period of January 11–26, 1994. These observations were carried out under the terms of the extensive VLBI/GPS campaign, when VLBI stations made nearly continuous series of observations.

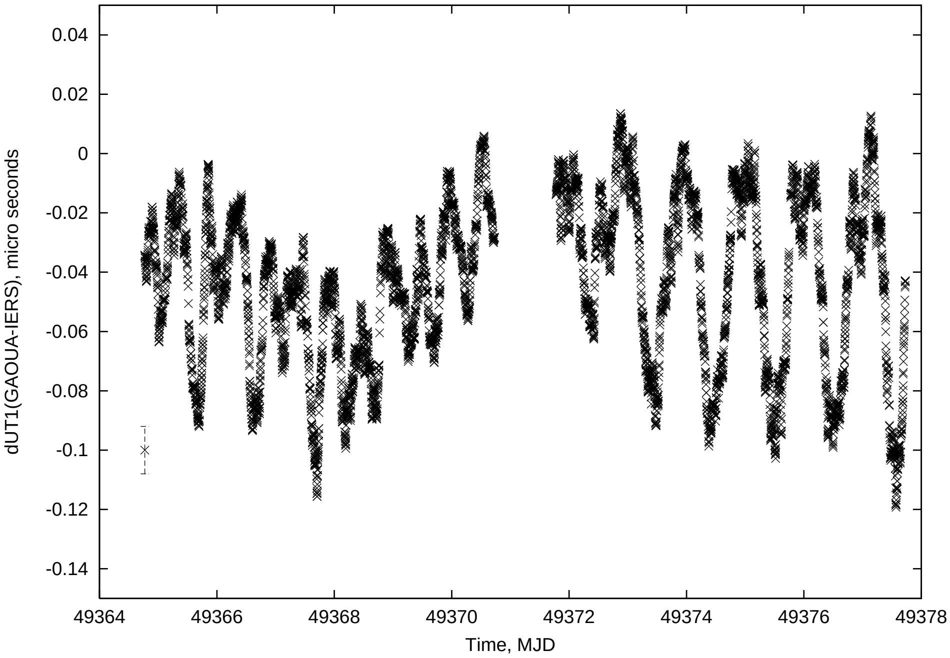

Figure 1: Estimated variations of the Earth rotation, $d(UT1-UTC)$

The procedure of data analyzing was the same as for the previous example with the exception: coordinates of sources and stations were fixed, the wet zenith delay and the clock offset were estimated as stochastic parameters, polar motion and Earth rotation were estimated as stochastic parameters with time propagation to ensure continuity in their behavior. The magnitudes of power spectral density of ruled white noise of estimated parameters were assumed to: for clock model: 18^2 ps^2/hour; for wet component of tropospheric delay: 1.0 cm^2/hour; for $d(UT1-UTC)$: 0.012^2 mts^2/hour; for dX and dY: 0.16^2 mas^2/hour.

This solution is based on the 27975 group delays. The 6279 estimations of the polar motion and the Earth rotation were obtained. The weighted rms post-fit residuals of this solution were equal to 10.2 ps. The estimated values of the Earth rotation variations are shown in Figure 1. The comparison of these estimations and Herring and Dong model is presented in Figure 2.

STEELBREEZE VER.2 SOFTWARE

The *SteelBreeze ver.1* software has had a set of limitations: it was written on the non-portable programming language, its design does not allow to extend it for analyzing additional geodynamical techniques, there are inner limitations in capacities of databases, which may cause to fail processing sessions with large set of observations (more then 15535). Due to these reasons in 1998 the developing of the *SteelBreeze ver.1* software was stopped and the new generation of the software was created. The new *SteelBreeze ver.2* software inherits all algorithms from previous version and expands them to overcome the limitations. However, there are some changes.

In new version the routine of data processing is carried out for selected time interval and does not depend on intervals of sessions; it makes possible to process sessions for overlapped time intervals. The algorithms of database manipulation are improved. New type of estimated parameters was added: "arc"; a parameter of this type is determined on selected time interval and does not depend on boundaries of a session. The graphic user interface is improved. A screenshot of the *SteelBreeze ver.2* software is shown in Figure 3.

The difference between version 1 and 2 of *SteelBreeze* software lies mostly in software developing technique. The *SteelBreeze ver.2* software is written on *C++*. It is executing on computers with different operating systems (Linux, FreeBSD, Solaris, *etc.*) and architecture (Intel, SPARCstation). It uses Qt user interface library. It is distributed under the GNU public license and its sources are available on the following URL:

$$http://sourceforge.net/projects/steelbreeze$$

for public access.

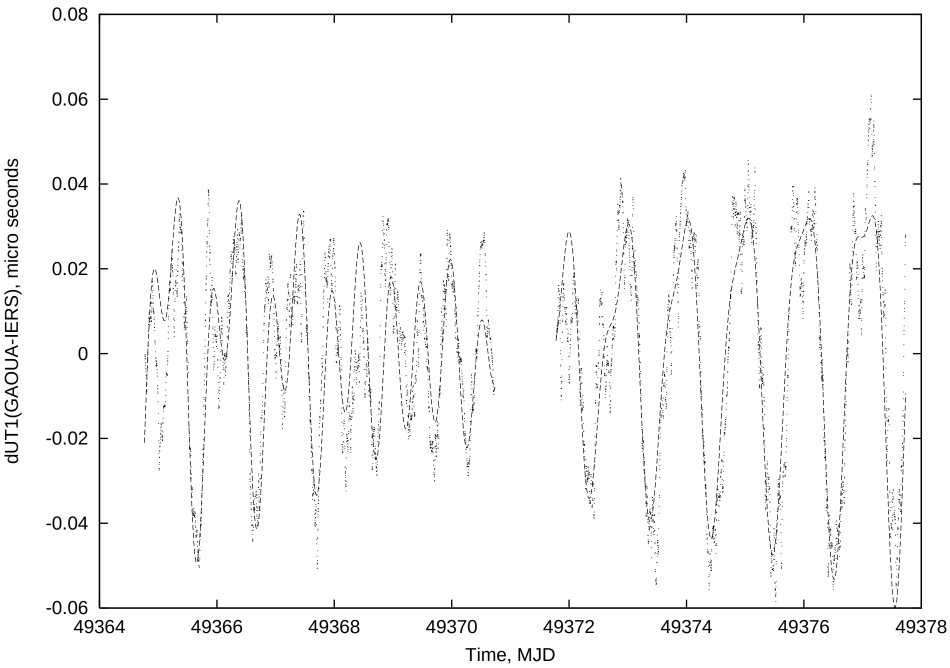

Figure 2: Subdaily variations in $d(UT1-UTC)$. The dots are the estimated values after elimination of long period variations. The dotted line is the variations in $d(UT1-UTC)$ according to Herring and Dong, 1993

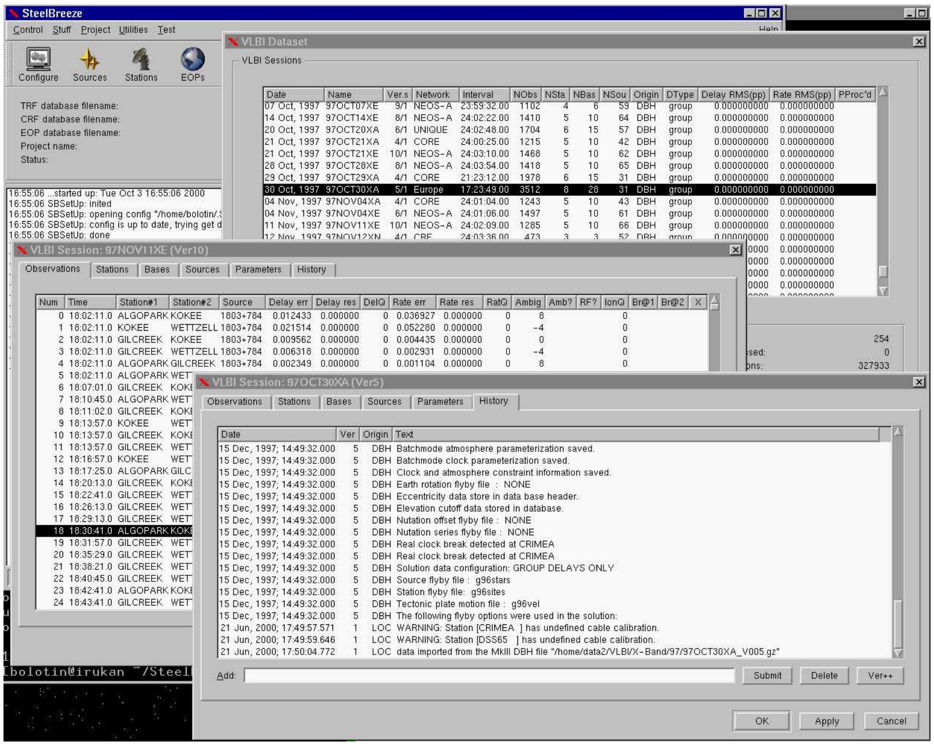

Figure 3: The screenshot of the *SteelBreeze ver.2* software

REFERENCES

[1] *Biermann G. J.* Factorization Methods for Discrete Sequential Estimation // Math. Sci. and Eng. Ser.–1977.–**128**.

[2] *Bolotin S.* Hight frequency variations of EOP from extensive VLBI operations in January 1994 // Proc. 2nd EVN/JIVE Symp.–1995.–P. 13–18.

[3] *Herring T. A.* // Proc. Symposium on Refraction of Transatmospheric Signals in Geodesy / Eds J. C. De Munch, T. A. Th. Spoelstra.–Netherland Geodetic Commision, Delft, Netherlands, Publications on Geodesy, 1992.–N 36.–P. 157–164.

[4] *Herring T. A. and Dong D.* Measurement of diurnal and semi-diurnal rotational variations and tidal parameters of Earth // J. Geophys. Res.–1994.–**99**.–P. 18051–18071.

[5] International Earth Rotation Service, IERS Conventions / Ed. D. D. McCarthy.–Paris, France, 1996.

[6] *Saastamoinen J.* Atmospheric Correction for the Troposphere and Stratosphere in Radio Ranging of Satellites // The Use of Artificial Satellite for Geodesy: Geophys. Monogr. Ser. / Eds S. W. Henriksen, *et al.*–AGU, Washington, D.C., 1972.–**15**.–P. 247–251.

[7] *Yatskiv Ya. S., Kur'yanova A. N., Medvedsky M. M.* Program Complex "Kiev-GR1" for Reduction of the VLBI Observations, Kiev, 1991.–preprint ITF-91-37R.

SEASONAL OSCILLATIONS OF THE POLAR MOTION DURING THE LAST FORTY YEARS

B. Kolaczek, J. Nastula

Space Research Centre, Polish Academy of Sciences
Bartycka 18A, 00-716, Warsaw, Poland
e-mail: kolaczek@cbk.waw.pl, nastula@cbk.waw.pl

Variations of seasonal oscillations of the polar motion during the last forty years are shown and discussed. Seasonal oscillations of the geodetic excitation functions of the polar motion were computed from the EOP (IERS) 97 C04 set of data together with their time variable spectra and correlations with the atmospheric excitation functions of the polar motion.

INTRODUCTION

Geophysical sources of amplitude variations of seasonal oscillations, *e.g.*, annual, semiannual and 120 days period of the polar motion are still not sufficiently known at the present level of accuracy of their determinations sub-miliarcseconds.

Variations of the polar motion are correlated with variations of the Effective Atmospheric Angular Momentum (EAAM) excitation function, but not so strongly as variations of length of day (LOD). Correlation coefficients between atmospheric and geodetic excitations of seasonal oscillations of the polar motion for the years of 1985–1996 to be equal to 0.5–0.6 were computed by Ponte [8]. This correlation coefficient is higher after considering the total atmospheric and oceanic angular momentum (OAM) [6, 8], but the models of the OAM are available only for the last few years.

The new improved reanalyses of EAAM data computed by the NCAR/NCEP (National Centers for Environmental Prediction/National Center for Atmospheric Research) for the last fifty years [9] enables studies of the correlation between geodetic and atmospheric excitation functions of the polar motion in such long period of time.

In the paper, the correlations of the EAAM and geodetic excitation functions of seasonal oscillations of the polar motion computed for the last forty years are discussed.

ANALYSES

Variations of seasonal oscillations of the polar motion

Applied here the EOP (IERS) 97 C04 pole coordinates data were divided by using the Butterworth band pass filter into two spectral bands, namely annual frequencies (500–300 days) and semiannual frequencies (250–150) days.

The Chandler, annual and semiannual oscillations were filtered from these data by the Fourier Transform Band Pass Filter (FTBPF) with the parameter λ giving a high frequency resolution [3, 5] (Figs. 1, 2). Variations of the amplitude of the annual oscillation are not so big as of the Chandler one; anyhow they are of the order of several tens of miliarcsecond (Fig. 1).

Semiannual oscillation of the polar motion is beating with the semi-Chandler one with the period of about 6–7 years. This combined oscillation achieves the maximum amplitude of the order of 10 mas [4]. They are separated by using the narrow FTBPF [3, 5] (Fig. 2). The amplitude of the semiannual oscillation itself is of the order of 6 mas in maximum. Slow variations of its amplitude are of the order of 1–2 mas. The amplitude of semi-Chandler oscillation is changeable.

Amplitudes of the 120 days oscillations are strongly variable reaching 4–5 mas in maxima [1, 2].

Geodetic and atmospheric excitation functions

The commonly used technique for comparing the polar motion excitation function with EAAM excitation function is as through determination of the so-called geodetic polar motion excitation function χ_1, χ_2 using time domain deconvolution formula [10]. The EOP (IERS) 97 C04 set of polar coordinate data were applied

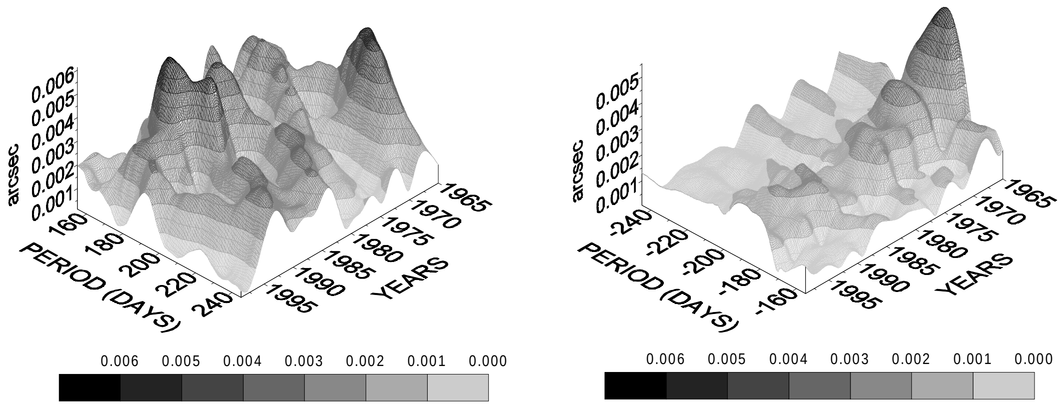

Figure 2: Semi-Chandler and semiannual oscillations of the EOP (IERS) 97 C 04 set of polar motion filtered by the FTBPF with $\lambda = 0.0005$

for computations of the geodetic polar motion excitation function for the period of 1962–1999. The Chandler period of 435 days and the dumping coefficient Q to be equal 100 were adopted for those determinations. The mentioned above reanalyses data EAAM of excitation functions were averaged over 1-day for consistency with the geodetic ones. The geodetic and atmospheric excitation functions for polar motion were divided by the use of the Butterworth band pass filter into three spectral bands, namely annual frequencies (450–230 days), semiannual frequencies (230–150 days), and 120 days oscillations frequencies (150–90 days).

The time variable spectra of the geodetic polar motion excitation functions of seasonal oscillations computed by the FTBPF are shown in Fig. 3. In the case of the annual oscillation a retrograde part of the spectra indicate ellipticity of the annual oscillation. The amplitude of the annual oscillation reached the maximum in the late of seventies and since this time it has been diminished. The amplitude of semiannual oscillation of the geodetic excitation function of polar motion, which is ten times weaker than annual one, is also elliptical (Fig. 3) what is proved by the retrograde part of this spectrum. There are three maxima of the amplitude of the semiannual oscillation around 1970, 1985–1987 and 1993–1995 years. They can be caused by El Nino phenomena.120 days oscillation of geodetic excitation function of polar motion is a very weak. High amplitudes of seasonal oscillations in the retrograde parts of the geodetic excitation function of polar motion in sixties and at the beginning of seventies are probably caused by the low accuracy of the considered data at this time.

Variations of time variable spectra of seasonal oscillations of the EAAM excitation functions of polar motion (not shown here) have a very similar character to the variations of the geodetic excitation functions [7]. The similarity of variations of geodetic and EAAM excitation functions of seasonal oscillations of polar motion is shown by computations of their correlations.

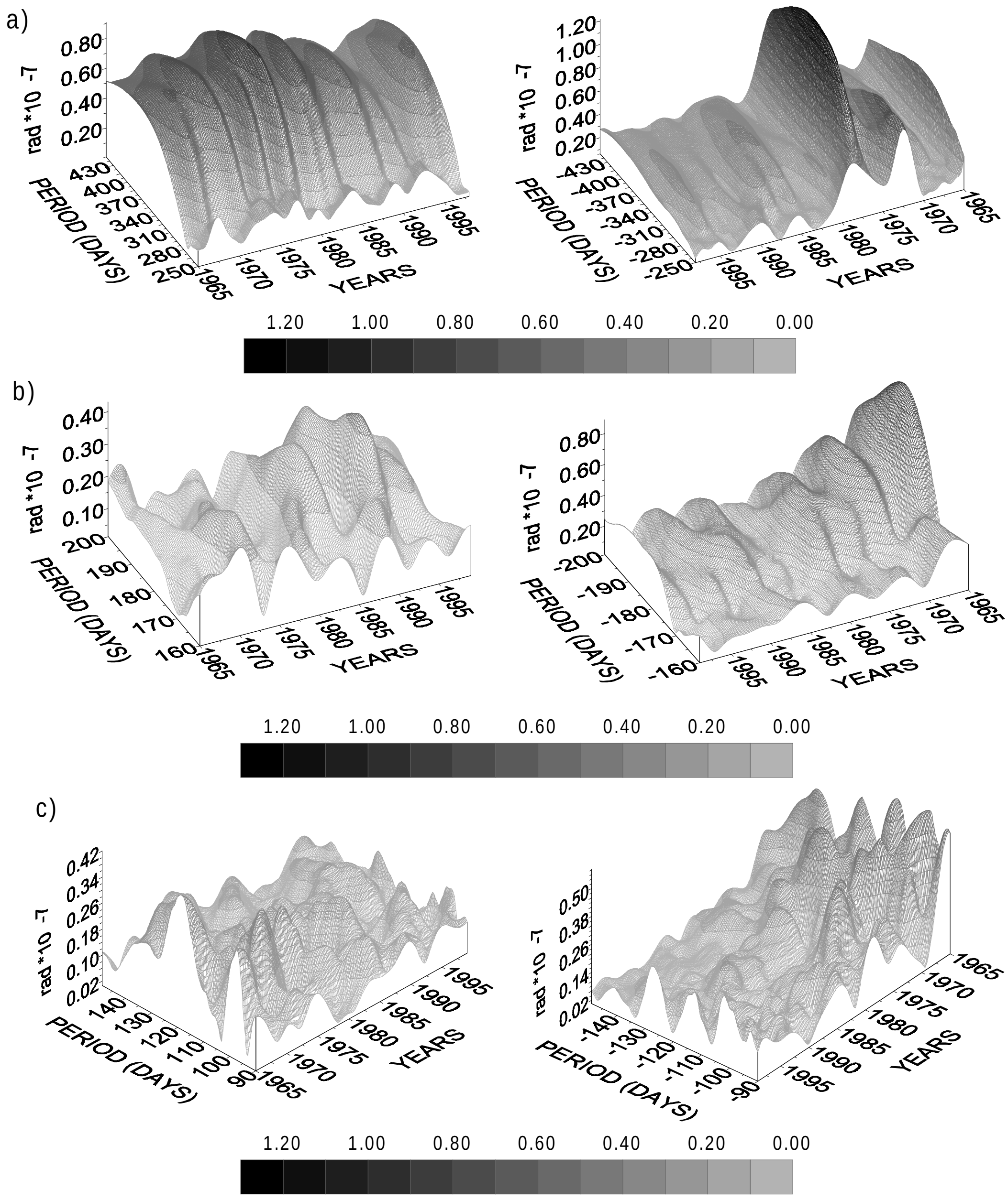

Figure 3: Time variable amplitude spectra of (a) annual, (b) semiannual, (c) 120 days oscillations of complex equatorial components of the geodetic polar motion excitation function filtered by the FTBPF with $\lambda = 0.001$ for the annual and with $\lambda = 0.0005$ for semiannual and 120 days oscillations, for the prograde (positive) and retrograde (negative) parts of spectrum

Correlations

Correlation coefficients between complex-valued components of geodetic and atmospheric functions of polar motion were computed since 1962 over 2190, 1095, 720, 540 days long intervals, with 100 days step for annual, semiannual, 120 days and subseasonal (shorter than 90 days) bands, respectively (Fig. 4). On the basis of the computed autocorrelation functions of all filtered data the estimated numbers of independent points are 33 and 128, for the seasonal and subseasonal bands, respectively. Using the standard Student-table for the 95 per cent confidence level we obtained critical values of the correlation coefficient equal to 0.31 and 0.17, respectively.

It is clear that the correlation has improved since 1970's for annual and semi-annual bands while only since 1980's for the subseasonal one. The correlation coefficient in the case of the annual oscillation is stable and

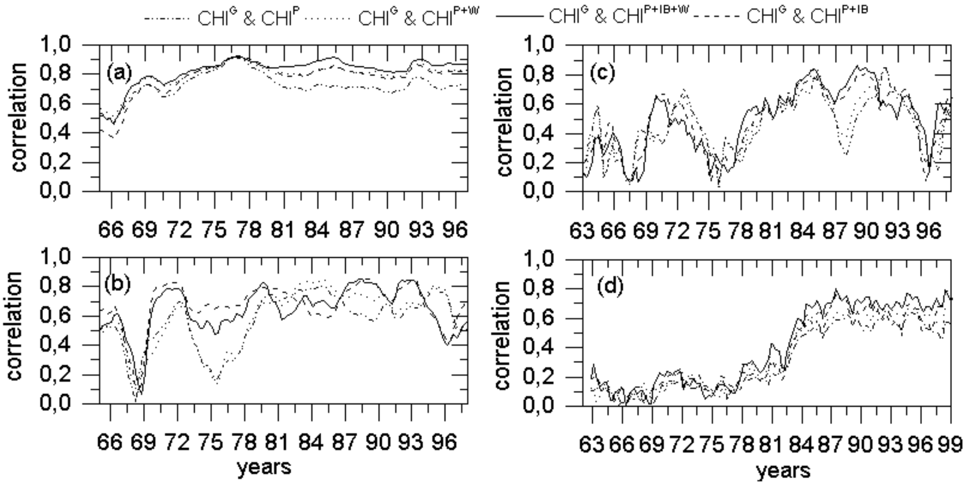

Figure 4: Correlation coefficients between the complex-valued equatorial components of geodetic and atmospheric excitation functions for polar motion separated by the Butterworth band pass filter into (a) 450–230 days, (b) 230–150 days, (c) 150–90 days, (d) 90–10 days bands

quite high, above 0.8, since 1970. In the case of semiannual oscillations these coefficients are changeable in the range of 0.6–0.8 since 1980. In the 120 days oscillation band the correlation coefficient is more stable only in the years 1980–1993. The IB correction, introduced to the pressure term of the atmospheric excitation function, increases the correlation somewhat but does not change a general tendency. Such a behaviour of the correlation coefficients is likely due to less accurate polar motion or atmospheric data before the mentioned years. Thus, the accuracy of estimates of geodetic and atmospheric excitation functions of polar motion before 1970's and 1980's still remains a matter of concern.

Acknowledgements. The researches reported here were supported by the project of the Polish Commitee Scientific Research, the Grant N 152/T12/97/13. The computation of the FTBPF time variable spectra were carried out by using the Kosek's computation routines.

REFERENCES

[1] *Kolaczek B.* Variations of Short Periodical Oscillations of Earth Rotation // Developments in Astrometry and their impact on astrophysics and geodynamics: Proc. 156th IAU Symp., Shanghai, China, Sept. 15–19, 1992 / Eds I. I. Mueller, B. Kolaczek.–Kluwer Academic Publishers, Dordrecht/Boston/New York.–1992.–P. 291–296.

[2] *Kolaczek B.* Short period variations of Earth rotation // Systemes de Reference Spatio–Temporels: Proc. Journees 1995.–1995.–P. 147–154.

[3] *Kosek W.* Time variable band pass filter spectrum of real and complex-valued polar motion series // Artif. Satell., Planetary Geodesy.–1995.–**30(1)**.–P. 27–43.

[4] *Kosek W., Kolaczek B.* Semi-Chandler and Semiannual Oscillations of Polar Motion // Geophys. Res. Letts.–1997.–**24**, N 17.–P. 2235–2238.

[5] *Kosek W., Popiński W.* Comparison between the Fourier transform band pass filter and the wavelet transform spectro-temporal analyses on Earth Rotation Parameters and their excitation functions // IERS Technical Notes.–1999.–N 28.–submitted.

[6] *Nastula J., Ponte R. M.* Further Evidence for oceanic excitation of polar motion // Geophys. J. Int.–1999.–**130**.–P. 469–474.

[7] *Nastula J., Kolaczek B.* Seasonal oscillations in regional atmospheric excitation of polar motion // Adv. Space Res.–2000.–submitted.

[8] *Ponte R. M. Stammer D., Marshall J.* Oceanic signals in observed motions of the Earth's pole of rotation // Nature.–1998.–**391**.–P. 476–479.

[9] *Salstein D. A., Kann D. M., Miller A. J., Rosen R. D.* The Sub-Bureau for Atmospheric Angular Momentum of the International Earth Rotation Service: A meteorological data center with geodetic applications // Bull. Amer. Meteorol. Soc.–1993.–**74**.–P. 67–80.

[10] *Wilson C. R.* Discrete polar motion equations // Geophys. J. Roy. Astron. Soc.–1985.–**80**.–P. 551–554.

THE GAOUA SERIES OF COMPILED CELESTIAL REFERENCE FRAMES

O. Molotaj[1], V. Tel'nyuk-Adamchuk[1], and Ya. Yatskiv[2]

[1] *Astronomical Observatory, Taras Shevchenko National University*
3 Observatorna St., 04053 Kyiv-53, Ukraine
e-mail: molotaj@observ.univ.kiev.ua

[2] *Main Astronomical Observatory, NAS of Ukraine*
27 Akademika Zabolotnoho St., 03680 Kyiv, Ukraine
e-mail: yatskiv@mao.kiev.ua

The GAOUA series of compiled celestial reference frames is obtained by using the original Kyiv arc length approach for combination of initial RSC solutions which are yearly submitted to the IERS CB by various VLBI Analysis Centers. The presentation is concerned with an analysis of accuracies of these individual and combined solutions and that of the ICRF.

KYIV ARC LENGTH METHOD

The history of the GAOUA (acronym used by the IERS to designate the Main Astronomical Observatory of NASU) series begins since 1989 when Y. Yatskiv and A. Kur'yanova [5] proposed and realized new approach to combine individual VLBI solutions. This approach combines a geometrical arc length method with a statistical evaluation of uncertainties of individual and compiled catalogues. The following items explain essentials of the approach (corresponding mathematical formulas can find in [2]):

- selection of "basic" catalogues of radio source (RS) positions as part of all the collected individual ones;
- search for defining RSs which are common for the selected "basic" catalogues;
- calculation of arc lengths (below simply "arcs") between all common defining RSs in each basic catalogue;
- intercomparison of the arcs for all basic catalogues, evaluation of catalogue weights, and determination of mean values of the arcs and "arc minus mean arc" residuals;
- construction of individual rigid frames based on the arcs and defined by positions of two selected RSs;
- construction of a combined rigid frame using the data of previous steps;
- alignment of this combined rigid frame to a standard celestial reference frame (the ICRF) and construction of a compiled reference frame under the following conditions: absence of a net rotation; minimum displacements among common RSs of the standard and compiled frames;
- extension of the reference frame realized by common defining RSs to the rest of RSs, involved in the process of constructing the compiled frame.

CONSTRUCTION OF THE GAOUA SERIES OVER 1997-2000

By using this method the 12 combined solutions were prepared in Kyiv on base of the individual solutions submitted to the IERS CB during 1989–2000 span (see [1], or of the recent publication [4]). Table 1 gives overview on the combined catalogues since 1997 when the RSC(WGRF)95 R 01 solution, known currently as the ICRF, was prepared by the IAU WGRF [1]. The Kyiv solutions obtained before 1996 were aligned to positions of the 23 primary RSs selected by the IERS and thus they are not included in Table 1. The frames are ordered as follows: basic frames, other ones, and compiled frame obtained. A calculation procedure follows the steps described above. Some distinctions were due to a number of common defining RSs. The more this number, the more is number of celestial zones, selected to adjust the rigid frame with the ICRF. Moreover, the different pairs of selected RSs were used to construct the rigid frames defined by this pair of RS. This circumstance is not critical because, in principle, any RSs' pair can be used in the method.

CONCLUSIONS

Analysis of results obtained gives a possibility to make the next conclusions:

Table 1: **List of VLBI frames used to construct the GAOUA compiled series over 1997–2000**. N is the number of RSs in a frame; N_d is the number of the defining RSs, which are common for the basic frames; σ_α and σ_δ are the averaged uncertainties in *mas* for right ascension and declination, respectively; W is the weight of the basic frame used for the rigid frame constructing; $\bar{\Delta\alpha_*}$ and $\bar{\Delta\delta}$ are the mean differences in terms of "Frame – ICRF" calculated for 212 defining RSs; $|\Delta\alpha_*|$ and $|\Delta\delta|$ are the m.r.s. of those differences

Frame	N	N_d	σ_α	σ_δ	W	$\bar{\Delta\alpha_*}$	$\bar{\Delta\delta}$	$\lvert\Delta\alpha_*\rvert$	$\lvert\Delta\delta\rvert$
a) 1997									
RSC(USNO) 95 R 04	556	27	0.07	0.08	0.57				
RSC(GSFC) 95 R 01	550	27	0.12	0.09	0.33				
RSC(JPL) 95 R 01	287	27	0.14	0.21	0.03				
RSC(NOAA) 95 R 01	249	27	0.18	0.25	0.07				
RSC(GIUB) 95 R 01	89	5	0.17	0.24	–				
RSC(SHA) 95 R 01	45	3	0.06	0.08	–				
RSC(GAOUA)97 C 01	598	212	0.15	0.18	–	.00	.20	.27	.31
b) 1998									
RSC(USNO)97 R 08	615	82	0.15	0.18	0.36				
RSC(GSFC)97 R 01	600	82	0.14	0.18	0.49				
RSC(JPL)97 R 01	287	82	0.20	0.28	0.15				
RSC(GIUB)97 R 01	266	26	0.78	0.59	–				
RSC(GAOUA)97 R 01	129	17	0.21	0.38	–				
RSC(GAOUA)98 C 01	631	212	0.11	0.13	–	.00	.00	.24	.26
c) 1999-1									
RSC(USNO) 98 R 01	640	187	0.14	0.16	0.69				
RSC(GIUB) 98 R 01	580	187	0.18	0.21	0.22				
RSC(JPL) 98 R 01	522	187	0.46	0.52	0.09				
RSC(GAOUA)98 R 01	198	54	0.24	0.41	–				
RSC(GAOUA)99 C 01	655	212	0.11	0.12	–	–.01	–.05	.32	.30
d) 1999-2									
RSC(GSFC) 99 R **	644	187	0.11	0.14	0.41				
RSC(USNO) 98 R 01	640	187	0.14	0.16	0.39				
RSC(GIUB) 98 R 01	580	187	0.18	0.21	0.15				
RSC(JPL) 98 R 01	522	187	0.46	0.52	0.06				
RSC(GAOUA)98 R 01	198	54	0.24	0.41	–				
RSC(GAOUA)99 C 02	673	212	0.08	0.09	–	.00	–.04	.26	.28
e) 1999-3									
RSC(SHA) 99 R 01	720	205	0.15	0.18	0.09				
RSC(USNO) 99 R 01	652	205	0.12	0.14	0.46				
RSC(GSFC) 99 R **	644	205	0.11	0.14	0.25				
RSC(GIUB) 99 R 01	602	205	0.15	0.17	0.20				
RSC(IAA)99 R 01	506	82	0.46	0.56	–				
RSC(FFI)99 R 01	431	58	0.16	0.12	–				
RSC(GAOUA)99 C 03	726	212	0.06	0.07	–	.00	.00	.23	.27
f) 2000									
RSC(SHA) 00 R 01	636	204	0.15	0.18	0.30				
RSC(GSFC) 00 R 01	624	204	0.11	0.13	0.42				
RSC(BKGI) 00 R 01	621	204	0.15	0.17	0.28				
RSC(IAA)00 R 03	312	81	0.13	0.20	–				
RSC(GAOUA) 00 R 01	191	47	0.22	0.39	–				
RSC(FFI)00 R 01	104	41	0.13	0.11	–				
RSC(GAOUA)00 C 01	669	212	0.07	0.08	–	.00	.01	.24	.26

$\Delta\alpha_* = \Delta\alpha \cdot \cos\delta$; ** – this frame is obtained directly from the GSFC

Table 2: **Rotational angles** $A1$, $A2$, and $A3$ of VLBI initial frames' axes to align its to those of the RSC(GAOUA)00 C 01 solution. The angles are calculated for common RSs of Table 1. σ is the averaged m.r.s. error of angles; all values in *mas*

Frame	$A1$	$A2$	$A3$	σ
RSC(SHA) 00 R 01	0.023	0.000	–0.014	0.008
RSC(GSFC) 00 R 01	0.008	0.023	0.003	0.008
RSC(BKGI) 00 R 01	0.021	0.009	–0.033	0.008
RSC(IAA)00 R 03	0.028	–0.004	0.154	0.043
RSC(GAOUA) 00 R 01	4.150	0.250	–0.045	0.120
RSC(FFI)00 R 01	0.023	–0.120	–0.760	0.120

- Uncertainties in right ascension are systematically better than those in declination for all Analysis Centers except for the FFI.
- Precision of the GAOUA series improves more than twice when uncertainties of initial frames improve only in 20 per cents. Likely, this peculiarity is connected with accumulation of observations.
- Two of the basic individual catalogues, the USNO and GSFC, have the same accuracy and during this span they have maximal weights. The weights of the basic solutions of other institutions are less more than twice except the last year. The GIUB solutions systematically differed a valuable rigid rotation with order of 0.5 mas around the ICRF. The BKGI solution has not this peculiarity (see Table 2 and tables in former papers).
- Axes of all GAOUA solutions align to those of the ICRF with accuracy 0.021 mas based on all 212 common defining radio sources.
- Comparisons between GAOUA solutions and the ICRF give zero mean differences in right ascension. Behavior of declination differences is more complex. While for the RSC(GAOUA)97 C 01 the big difference is explained by the effect of tropospheric gradient, not taken into account in some initial frames at 1995, one can see that the difference grows in the two first solutions of 1999. This effect can be introduced by the different subsamples of the ICRF sources used in the arc method. Thus, in Table 3 the defining RSs are listed with the differences more than 0.6 mas in any coordinate between last Kyiv solution RSC(GAOUA)00 C 01 and RSC(WGRF)99 R 01 (the ICRF–Ext–1). Almost all these RSs except 1604-333 have been registered already as those with big differences "RSC(GAOUA)99 C 03 – RSC(WGRF)99 R 01". Additional calculation were carried out to clear up the question on influence of errors of initial catalogues on the combined solution. The result is that only deviations of three southern RSs (0629-418, 1604-333, and 1718-649) can be explained by this manner.

Table 3: **List of large positional differences of the defining RSs** in terms of "RSC(GAOUA)00 C 01 – RSC(WGRF)99 R 01". σ_α and σ_δ are the GAOUA uncertainties; all values in *mas*

RS Designation	$\Delta\alpha$	σ_α	RS Designation	$\Delta\delta$	σ_δ
1604-333	+0.94	0.64	1604-333	–0.78	0.22
2312-319	–0.60	0.20	2312-319	–1.13	0.24
0138-097	+1.64	0.10	0440-003	–1.08	0.09
1143-245	–0.87	0.09	0458+138	–0.84	0.29
1448+762	+0.88	0.24	0812+367	+0.71	0.07
			1616+063	–0.61	0.13
			2059+034	–0.66	0.09

Acknowledgements. Authors are grateful to the staff of the Central Bureau of the IERS as well as to Dr. Chopo Ma (GSFC) for providing us the initial VLBI reference frames used in this work.

REFERENCES

[1] 1998 IERS Annual Report.–Central Bureau of IERS, Observatoire de Paris, Paris.–1999.

[2] *Kur'yanova A. N., Yatskiv Ya. S.* The compiled catalogue of positions of extragalactic radio sources RSC(GAOUA)91 C 01 // Kinematics and Physics of Celestial Bodies.–1993.–**9**, N 2.–P. 15.

[3] *Ma C., Arias E. F., Eubanks T. M., et al.* The International Celestial Reference Frame realized by VLBI // IERS Technical Note 23. Definition and Realization of the International Celestial Reference System / Eds C. Ma and M. Feissel.–Central Bureau of IERS, Observatoire de Paris, Paris, 1997.–P. II-3.

[4] *Molotaj O. A.* Celestial Reference Frame RSC(GAOUA)99 C 03 // IVS General Meeting Proceedings, NASA/CP-2000-209893.–2000.–P. 338.

[5] *Yatskiv Ya. S., Kur'yanova A. N.* A new approach to the construction of a compiled catalogue of positions of extragalactic radio sources // Inertial Coordinate System on the Sky: Proc. 141th IAU Symp.–Leningrad, Kluwer, 1990.–P. 295.

REFINEMENT OF LINKING OPTICAL/RADIO REFERENCE FRAMES ON THE BASIS OF POSITIONAL OBSERVATIONS CONDUCTED IN UKRAINE, CHINA AND RUSSIA

G. Pinigin[1], A. Shulga[1], N. Maigurova[1], Yu. Protsyuk[1], W. Jin[2], Zh. Tang[2], Sh. Wang[2], F. Velichko[3], P. Fedorov[3], R. Gumerov[4], I. Bikmaev[4]

[1] *Mykolaiv Astronomical Observatory, Mykolaiv, Ukraine*

[2] *Shanghai Astronomical Observatory, Shanghai, China*

[3] *Astronomical Observatory, Kharkiv National University, Kharkiv, Ukraine*

[4] *Engelhardt Astronomical Observatory, Kazan State University, Kazan, Russia*

Preliminary results of cooperative programme for refinement of linking optical/radio reference frames are discussed. The instrumentation, methods of observations and reductions as well as preliminary results are presented. Optical positions of several extragalactic radio sources (ERS) are determined by using the CCD telescopes of China, Russia and Ukraine. The catalogue, which consists of 14000 stars selected from the USNO–A2.0 in the fields around 200 ERS is used as reference one. The positions of stars in this catalogue were obtained from observations with Mykolaiv Axial meridian circle (AMC) for declination zone from equator to +70° in the 11–14.5 magnitude range made during 1996–1998. It is estimated that an expected accuracy of the optical/radio linking in case of using about 200 ERS for northern declination zone is on the level of 5 mas provided the uncertainties ERS optical positions are not worse than 20 mas.

INTRODUCTION

The HC is considered as a best realization of the ICRF in optical frequency range. The equatorial axes of the HC have been satisfactory agreed relative to the ICRF at the epoch 1991.25 with an accuracy of ± 0.6 mas. However, the Hipparcos frame will lose this link progressively due to uncertainties of the Hipparcos proper motions. It is necessary to verify and check this link for variation with time. However, the link of HC to the ICRF in magnitude range above 10 mag is not easy. There are several ways for such check, and some of them could be realized by using the CCD astrographs and automatic meridian telescopes (AMT) (Argue, 1991; Kovalevsky, 1995; Stone, 1996; 1997). Proposed link programme could provide an intermediate system of reference stars in the HC system made with AMC in fields around ERS selected. Cooperative CCD telescopes with available FOV and sensitivities should guaranty a sufficient amount of intermediate reference stars for the determination of precise positions of faint ERS as well as to cover a magnitude range between intermediate stars and ERS optical counterparts. This cooperative programme is elaborated on the basis of joint research work in the field of optical/radio linking between Mykolaiv Astronomical Observatory (Ukraine) and Shanghai Astronomical Observatory (China) started in 1996 (Tang *et al.*, 2000).

The primary task of the proposed cooperative programme is establishment of optical/radio linking with accuracy better than 5 mas globally. It will be appropriate for enhancing a current link accuracy. From equations (1) it can be shown that for some available accuracy of ERS optical positions and for enough number of ERS it is possible to have a high accuracy of optical/radio linking (Fig. 1):

$$\begin{aligned} \Delta\alpha_{O-R} &= \mathrm{tg}\delta(u\cos\alpha + v\sin\alpha) + w, \\ \Delta\delta_{O-R} &= -u\sin\alpha + v\cos\alpha, \end{aligned} \tag{1}$$

where $\Delta\alpha_{O-R} = \alpha_O - \alpha_R$, $\Delta\delta_{O-R} = \delta_O - \delta_R$ are coordinate differences of ERS in optical and radio reference frames; u, v, w is rotation angles about the x, y, z axes, respectively.

It can be shown on the basis of equations (1) that rotation parameters accuracy of 5 mas will be reached by using of about 200 ERS with positional accuracy not worse than 20 mas (Fig. 1).

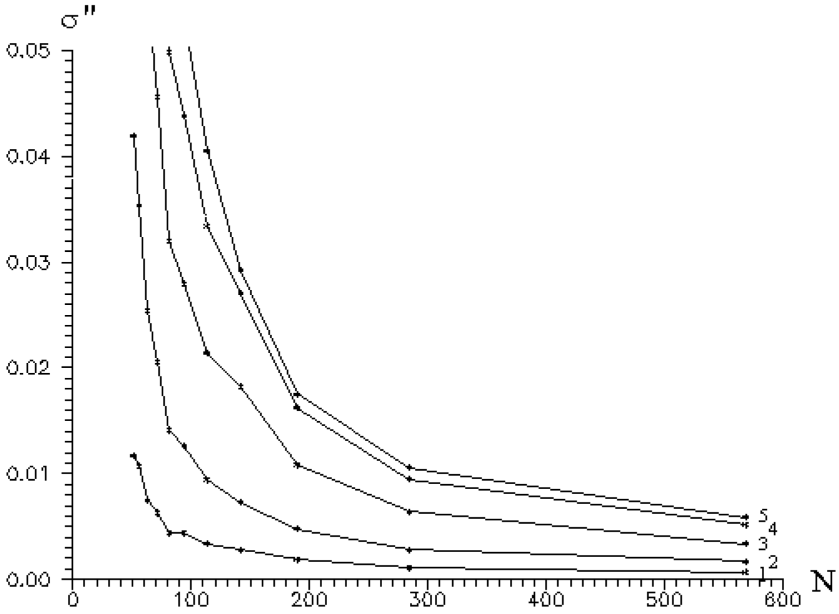

Figure 1: Rotation parameters accuracy (σ) in dependence of ERS number (N) and optical positions accuracy ($\epsilon_{\alpha,\delta}$: 1 – $\pm 0.''01$, 2 – $\pm 0.''02$, 3 – $\pm 0.''03$, 4 – $\pm 0.''04$, 5 – $\pm 0.''05$)

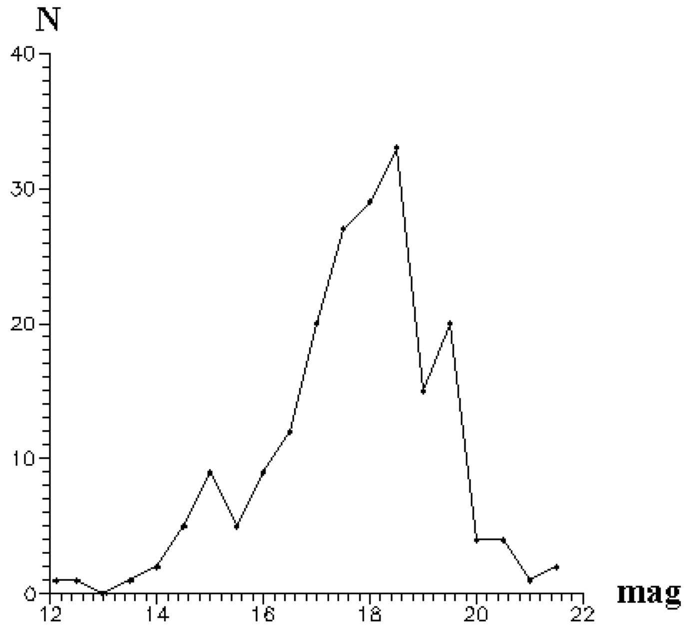

Figure 2: Distribution of selected ERS with the magnitudes in optical domain

PROGRAM AND INSTRUMENTATION

The cooperative program includes about 200 ERS for declination zone from equator to +70°. A distribution of selected ERS with the magnitudes in optical domain is shown in Fig. 2.

There are several cooperative CCD telescopes used in the program: AMC – Axial Meridian Circle (180, 2480) and Zone astrograph (160, 2044) of the Mykolaiv Astronomical Observatory (MAO) equipped by the similar CCD ISD017A (1040 × 1160, 16 × 16 mkm, $1''.6$/pix); AZT-8 astrograph (700, 2819)) of the Astronomical Observatory of the Kharkiv University (Ukraine) with the CCD ST-6 (375×241, 23×27 mkm, $1''.8 \times 2''.1$/pix); AZT-22 astrograph (1500, 11600) of the Engelghardt Astronomical Observatory of the Kazan University (Russia) installed in Turkey and equipped by the CCD ST-8 (1530 × 1020, 9 × 9 mkm, $0''.16$/pix) as well as 1.56 meter astrograph (1560, 15600) of the Shanghai Astronomical Observatory (China) with the CCD SONI (1024×1024, 16 × 16 mkm, $0''.25$/pix) (Maigurova *et al.*, 2000; Tang *et al.*, 2000) (see Table 1).

The Mykolaiv AMC was put into operation in 1995. AMC was equipped with CCD (256×288, 32 × 24 mkm) and computer control system. It permits to observe stars up to 14.5 limit magnitude. Observations of intermediate reference stars in the selected fields dimension $24' \times 60'$ around 200 north ERS and in the 11–14.5 magnitude range were made during 1996–1998. It was made about 120000 observations of 15000 stars including intermediate reference stars from USNO–A2.0 in selected fields, primary reference stars from HC and additional stars from TC. After installation on the AMC of a new CCD (ISD017A 1040 × 1160, 16 × 16 mkm, $1''.6$/pix) direct observations of bright counterparts of 24 ERS (up to 15 magnitudes) will be started in 2001.

Table 1: Cooperative telescopes used in programme

Telescope	AMC (Mykolaiv, Ukraine)	ZA (Mykolaiv, Ukraine)	AZT-8 (Kharkiv, Ukraine)	1.56 m ShAO (Shanghai, China)	AZT-22 (Antalia, Turkey)
Type	refract	refractor	reflector	reflector	reflector
Optical param D, F (mm)	180 2480	160 2044	700 2819	1560 15600	1500 11600
CCD	ISD017A 1040 × 1160 16 × 16 mkm $1''.26$/pix $23' \times 26'$	ISD017A 1040 × 1160 16 × 16 mkm $1''.6$/pix $28' \times 31'$	ST-6 375 × 241 23 × 27 mkm $1''.8 \times 2''.1$/pix $8' \times 10.5'$	SONI 1024 × 1024 16 × 16 mkm $0''.25$/pix $4' \times 4'$	ST-8 1530 × 1020 9 × 9 mkm $0''.16$/pix $4' \times 3'$
Mode	drift scan	drift scan, stare	stare	stare	drift scan, stare
Magnitude range	$10^m \div 16^m$	$12^m \div 15^m$	$15^m \div 17^m$	$17^m \div 19^m$	$19^m \div 21^m$
Observation program	24 ERS; refer. stars in selected fields (200 ERS)	20 ERS	65 ERS	75 ERS	50 ERS

By using some CCD astrographs direct observations of ERS for astrograph limiting magnitudes were started from 1998–99: with Mykolaiv ZA about 20 ERS in magnitude range $12^m \div 15^m$; with Kharkiv AZT-8 65 ERS in magnitude range $15^m \div 17^m$; with Shanghai 1.56 meter astrograph about 75 ERS in magnitude range $17^m \div 19^m$ and with AZT-22 astrograph of Kazan University about 50 ERS in magnitude range $19^m \div 21^m$.

3. REDUCTION AND RESULTS

3.1. AMC catalogue of reference stars

The intermediate version of AMC catalogue (AMC1B) is available via WWW:
http://mypage.goplay.com/naom/amc1b.zip.
It contains about 15000 stars with catalogue accuracy on both coordinates:

$$\epsilon_\alpha \cos\delta = \pm 0''.079 \cdot (\sec Z)^{0.32} \cdot (\mathrm{mag} - 7)^{0.20};\ \epsilon_\delta = \pm 0''.093 \cdot (\sec Z)^{0.12} \cdot (\mathrm{mag} - 7)^{0.18}.$$

3.2. First estimation of ERS optical/radio differences

For small fields of view (FOV) of CCD telescopes one can consider influences of all distortions as negligible and, therefore, can adopt a linear model of reduction for:

a) the Kharkiv astrograph

$$X = ax + by + cxy + d,$$
$$Y = ex + fy + gxy + h, \tag{2}$$

where X, Y are standard coordinates; x, y are the measured coordinates.

Comparison between optical and radio positions is presented in Table 2 for several selected ERS. An accuracy of optical/radio ERS position differences obtained by using the AMC reference stars catalogue is given (in arcsec).

Table 2:

ERS	mag	number	$\Delta\alpha_{O-R}$	$\sigma_\alpha \cdot \cos\delta$	$\Delta\delta_{O-R}$	σ_δ
0735+178	16.2	5	0.87	±0.02	0.10	±0.04
0248+430	17.6	6	0.27	0.02	0.10	0.04
2200+420	14.7	7	–1.76	0.01	0.17	0.04
0738+313	16.1	6	–0.10	0.02	0.20	0.02
1749+096	16.8	6	1.02	0.10	–0.78	0.12
2145+067	16.5	5	0.60	0.07	–1.09	0.02

b) the Shanghai astrograph

$$X - x = a_1 + a_2x + a_3y,$$
$$Y - y = b_1 + b_2x + b_3y, \tag{3}$$

where X, Y and x, y are above mentioned for equations (2).

Comparison between optical and radio positions is presented in Table 3 for some selected ERS (in arcsec).

Table 3:

ERS	mag	$\Delta\alpha_{O-R}$	$\sigma_\alpha \cdot \cos\delta$	$\Delta\delta_{O-R}$	σ_δ
0552+398	18.0	–0.10	±0.22	+0.03	±0.15
0735+178	16.1	–0.50	0.14	0.29	0.13
0818–188	15.0	0.20	0.16	–0.16	0.12
0827+243	17.3	–0.78	0.19	0.98	0.23
0851+202	15.4	–0.01	0.12	–0.40	0.14
1652+398	13.9	–0.08	0.16	0.72	0.16
1727+502	16.0	0.11	0.17	0.24	0.18
2145+067	16.5	0.42	0.15	0.77	0.15
2200+420	14.7	0.01	0.23	0.05	0.25

c) Comparison between optical and radio positions for ERS0735+178 obtained with Shanghai, Kharkiv and Kazan astrographs has showed a good agreement within random errors. Among these telescopes the Kazan AZT-22 has negligible systematic errors.

It is to be noted that accuracy of optical/radio ERS position differences is determined mainly by accuracy of intermediate reference stars positions. It is a main reason for large dispersion of optical/radio differences and random error, especially in case of using faint reference stars. Also, the low accuracy of data given in Table 3 may be explained by existence of systematic errors. From another side when ERS observation number will be of about 10–16 the expected mean accuracy should be about $0''.02$.

CONCLUSION

1. Determination of optical/radio ERS differences with position accuracy of 20 mas by using the observations of 200 ERS permits to determine rotation parameters with accuracy of 5 mas and to refine the optical/radio reference frames linking.

2. The expected accuracy is possible by using the cooperative telescopes provided sufficient number of ERS observations (not less than 10–16) and final position accuracy of AMC catalogue of intermediate reference stars on the level of not worse than 50 mas.

Acknowledgements. This work is partially supported by the Russian Foundation of Basic Research (Grant 99-02-17514).

REFERENCES

[1] *Argue A. N.* // Reference Systems: IAU Coll. N 127.–USNO.–1991.–P. 63.

[2] *Kovalchuk A., Pinigin G., Shulga A.* // Journees 1997 Systemes de reference Spatio-Temporels, Sept. 22–24, Prague, 1997.–P. 14–17.

[3] *Kovalevsky J.* // Astronomical and Astrophysical Objectives of SubMilliarcsecond Optical Astrometry: IAU Symp. N 166 / Eds E. Hog and R. Seidelmann.–Dordrecht: Kluwer Acad. Publ., 1995.–P. 127.

[4] *Maigurova N., Pinigin G., Shulga A., et al.* // Astrometry, Geodinamycs and Celestial Mechanics before XXI Century / Ed. A. Finkelstein.–Saint-Petersburg, 2000.–P. 133. (in Russian).

[5] *Stone R. C., et al.* // Astron. J.–1996.–**111**, N 4.–P. 1721–1742.

[6] *Stone R. C.* // Astron. J.–1997.–**114**, N 6.–P. 2811–2821.

[7] *Tang Z. H., Jin W. J., Wang S. H., et al.* // Towards Models and Constants for Sub-Microarcsecond Astrometry: IAU Coll. N 180 / Eds K. J. Johnston, *et al.*–USNO, USA, 2000.–P. 57.

Session 3. EAS's Observations

THE INFLUENCE OF TEMPERATURE AND HUMIDITY INVERSION ON CHANGE OF REFRACTION INDEX OF AIR AND CALCULATION OF RANGING CORRECTION TO EARTH ARTIFICIAL SATELLITES

I. Tegza

Space Research Laboratory, Uzhgorod State University
4 Daleka St., 88000 Uzhgorod, Ukraine

On basis of the aerological data, obtained at six stations of Ukraine in day- and night-time during a year, inversion of temperature t and of partial pressure of water vapour e in troposphere are investigated. The criterion of presence of inversion was the condition $(f_2 - f_1) \geq \Delta f$, where f_1 and f_2 are the measured parameters at lower and upper atmospheric layers, Δf – accuracy of measurement (or determination) of parameter f. Statistical data on inversions of t and e are given in Table 1. Inversions of t taking place in night occur about 2–3 time more often than in day, mainly at the expense of radiative inversions, which begins at the ground level. Inversions of t causes the corresponding inversions of e, but the place and the power (the thickness of layer) of these inversions do not always coincide. A majority of inversions of t and e in day are placed above the ground level. There are approximately the same quantity of inversions of e at day and night. Inversions of e causes the corresponding inversions of index refraction of water vapour N. The placing and the power of inversions of e and N are in good agreement. The range correction due to water vapour will be greater in case of existence of inversions of N. Results of wet range correction calculation both with inversions $(\Delta\rho)$ and without inversions $(\Delta\rho')$ are given in Table 2. In this table h_1 means the altitude, at which inversion begins, Δh is power of inversion, $\Delta e = e_2 - e_1$ and ΔN is inversion intensity of e and N, respectively. In Table 2 superscripts $^{1)}$ means Chernivci, night; $^{2)}$ means L'viv, night; $^{3)}$ means Kyiv, night. As one can see from Table 2, $\Delta\rho - \Delta\rho'$ is large, when Δe and corresponding ΔN are large. Also $\Delta\rho - \Delta\rho'$ increases, when Δh increases, although this dependence is not so evident. All calculations were done for zenith direction. The maximal contribution of inversion of e to range correction is 5 cm. This value is large enough because of the total wet range correction is equal to 20–40 cm in zenith direction. At larger zenith angles this contribution increases, but question arises whether we can use an assumption of spherical-symmetric atmosphere at large zenith angles.

Table 1: Statistical data of inversions of t and e

Station		number of dates	number of inversions		second layer inversions		ground level inversions	
			t	e	t	e	t	e
Kyiv	day	54	20	35	5	8	–	–
	night	140	59	61	6	14	7	2
Uzhgorod	day	53	7	19	1	2	–	–
	night	119	61	36	7	5	26	4
L'viv	day	63	19	27	–	4	–	–
	night	135	113	78	15	12	77	20
Shepetivka	day	32	17	19	1	4	2	–
	night	109	101	63	23	11	45	50
Chernivci	day	49	16	20	3	6	2	3
	night	104	92	61	21	12	75	38
Simpheropol	day	83	24	24	2	3	1	1

Table 2: Wet range corrections and characteristics of inversions at different dates

Date	h_1, km	Δh, km	Δe, mbar	ΔN	$\Delta\rho - \Delta\rho'$, m
23.03 [1)]	0.21	0.18	2.45	11.10	0.017
25.06 [1)]	0.21	0.30	5.91	14.33	0.039
26.05 [1)]	0.21	0.33	6.60	27.29	0.027
03.08 [1)]	0.21	0.45	8.04	30.28	0.034
16.10 [1)]	0.21	0.59	9.33	39.10	0.050
22.08 [1)]	3.88	0.06	0.45	2.30	0.002
15.05 [1)]	4.60	0.40	0.62	3.66	0.007
20.03 [2)]	0.33	0.17	0.82	3.79	0.009
26.03 [2)]	0.33	0.33	0.86	3.89	0.011
02.01 [2)]	1.26	1.14	1.27	6.84	0.025
02.11 [2)]	3.00	1.65	0.56	3.80	0.016
07.08 [2)]	4.00	1.00	1.02	6.10	0.030
02.02 [2)]	4.00	1.24	0.20	1.39	0.020
12.02 [2)]	4.50	0.90	0.35	2.24	0.013
10.09 [2)]	5.00	1.00	0.44	2.76	0.018
29.04 [3)]	0.50	0.17	1.32	6.30	0.037
18.05 [3)]	1.25	0.22	1.19	6.30	0.025
26.02 [3)]	4.00	1.00	0.06	0.48	0.005

EVOLUTION OF ORBITS OF GEOSTATIONARY OBJECTS AND PROBABILITY OF THEIR COLLISION

A. G. Kirichenko[1], L. M. Kizyun[2], V. U. Klimik[1]

[1] *Space Research Laboratory, Uzhgorod State University (SRL), Uzhgorod, Ukraine*
e-mail: `space@univ.uzhgorod.ua`

[2] *Main Astronomical Observatory, NAS of Ukraine*
27 Akademika Zabolotnoho St., 03680 Kyiv, Ukraine
e-mail: `kisyun@mao.kiev.ua`

A statistical dependence of change of 300 geosynchronous satellites semi-major axis with a launch time and so with a subsatellite longitude drift is presented. The computing a probability of collision of satellites in the geostationary ring is outlined.

The observations of high orbital objects the semi-major axis (a) of which are more than 20,000 km are still actual now. The monitoring of the geostationary ring performed by photographic method at MAO (Kyiv) and SRL (Uzhgorod) allow to determine the orbits and identify the objects [1, 2].

It is known that resonance perturbations in the satellite movement causes a longitude drift and a pendulum-like movement of satellite relative to the stable point of libration. The passive objects evolution takes place according to celestial mechanic laws. The orbital plane is precessing with a period of 52 years and amplitude of 15° [3].

A catalogue of geostationary objects [4] was used for study of satellites orbits evolution. The objects with $da = (a - 42164\ \mathrm{km}) > 100$ km are included for study. Fig. 1 presents the objects semi-major axis according to the year of their launches during the 35 years.

Here the dotted line is parabola approximation, which has been computed by the least square adjustment: $da = -6.671253\, r^2 + 26482.812\, r - 26281514.9$, where r is the date (year) of launch. A dependence between the satellite semi-major axis and longitude drift is straightforward: $da = -78.7471\lambda - 3.0436$ with a high correlation coefficient, $p = 0.99985$.

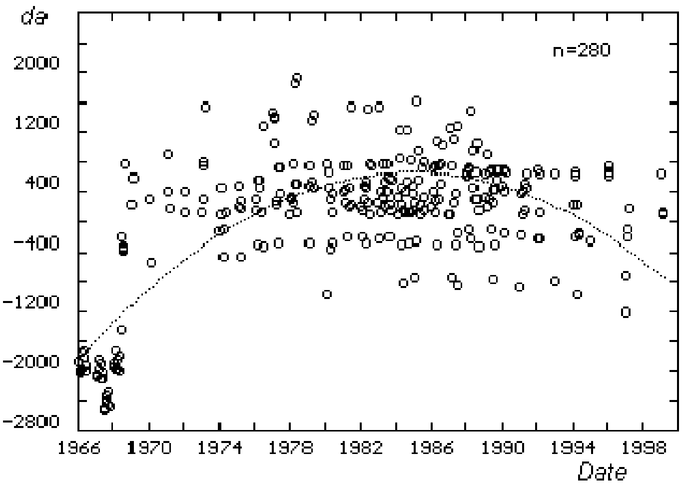

Figure 1: Change of objects semi-major axis according to the year of their launches

Dependences above mentioned show that the object's evolution is taken place. Up to 2017 year the geostationary objects of the first launches will reach the maximal angle of the orbital inclination to the equator. Only systematic positional observations of geostationary objects would allow this evolution to be investigated. After satellite identification the satellites should be enter to catalogue [1, 2]. However, there are objects having companions located closer than $0.1°-0.3°$ that are so-called "collocated" satellites. The catalogues analysis [4] showed that there are 140 "collocate" zones from $5°$ to $292°$, each of them have from 2 to 8 objects. That's why there is a possibility of the collisions. Figs. 2–3 show that the risk of such collision is large enough.

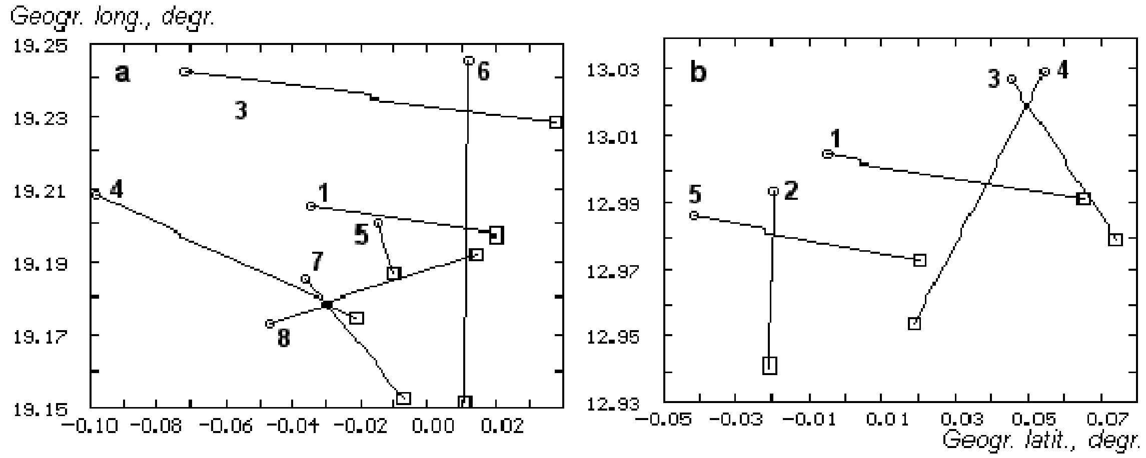

Figure 2: The movement of 8 geosynchronous satellites of Astra type (a) and 5 geosynchronous satellites of Hot Bird type (b) for 4 days in March 1999 (Uzhgorod). Circles-initial satellites positions, squares-final positions, figures-satellites numbers

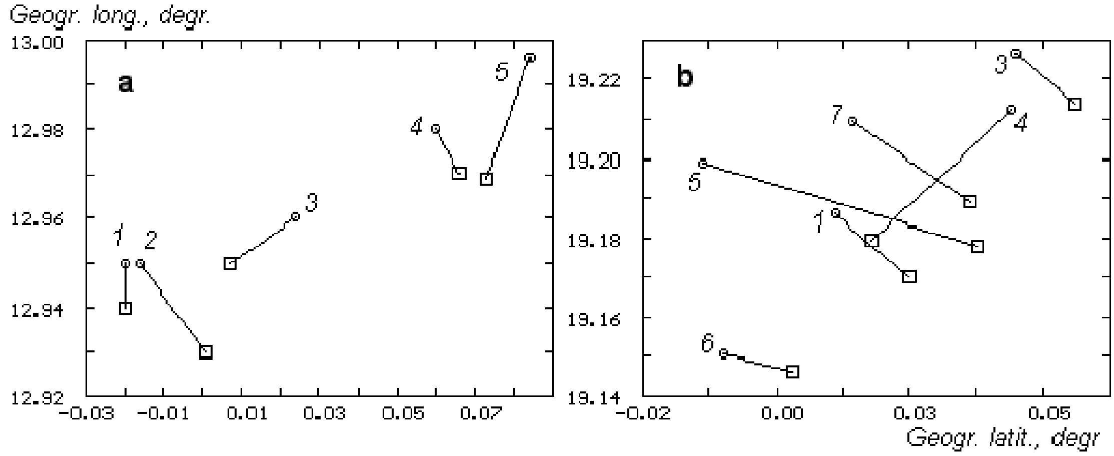

Figure 3: Geosynchronous satellites movements using the results of MAO (Kyiv) observations in January 1999 in two "collocation" zones: (a) for 1.1 day; (b) for 0.12 day

For investigation of the collisions risk the determinancy-probability method was used [5]. The probability p of two objects collision is determined as a product $p = p_{\varphi\lambda}\, p\,(\Delta h < R + r)$, where $p_{\varphi\lambda}$ is the probability of the collision under condition that the objects have the same height h upon the Earth, $p\,(\Delta h < R + r)$ is the probability that the difference distances of two satellites centres from the Earth Δh less than $R + r$, where R and r are the satellites radii.

It may be presented as:

$$p\,(\Delta h < R + r) = \int p\,(h) \left(\int_{h-(R+r)}^{h+(R+r)} p\,(x) dt \right) dh,$$

where $p\,(h)$ is the probability density of the objects distribution by the height.

The objects distribution by the height has a small difference from such one by the declination $p(\delta)$. The function $p(\delta)$ was obtained from 2982 observations at SRL for three years (Fig. 4), where δ – in km (1° corresponds to 750 km).

The observations at SRL and MAO are completed now for experimental determination of satellites distribution in the geostationary orbit.

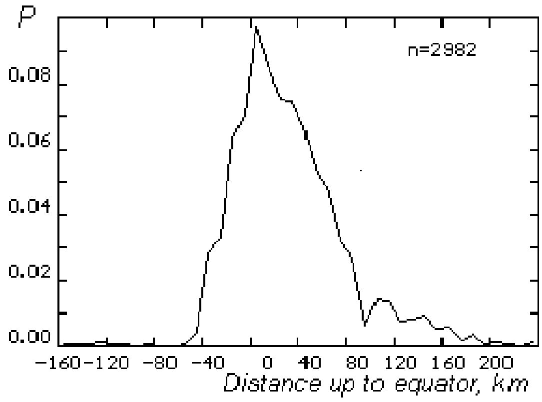

Figure 4: Density of distribution probability of the satellites equatorial distances

REFERENCES

[1] *Demchyk M. I., Kirichenko A. G., Kizyun L. M., et al.* Some results of observation and identification of geosynchronous space objects // Space Science and Technology, Supplement.–1996.–**2**, N 1.–52 p. (in Ukrainian and Russian).

[2] *Kizyun L. M., Kirichenko A. G., Rudenko S. P., et al.* Catalogue GOCKU96 of positions and orbital elements of geosynchronous space objects observed in 1996 // Space Sciense and Technology, Supplement.–1998.–**4**, N 1.–52 p.

[3] *Vershkov A. N., Grigoriev K. V., Sochilina A. S.* Explosions in the geostationary orbite: the modelling, estimate of the region movement fragments and the collision danger // Near Earth astronomy and problems of the small Solar system bodies study: Abstract for Sci. Conf.–Obninsk, IA RAN.–1999.–P. 21. (in Russian).

[4] Log of objects near the geostationary ring, Issue N 19, 20, 1999, ESA/ESOC.

[5] Collisions in the near Earth space (space debris) / Ed. A. G. Masevich.–Moscow: Kosmoinform, IA RAN, 1995.–P. 19–91. (in Russian).

SOME QUESTIONS OF THE IDENTIFICATIONS OF THE ARTIFICIAL SATELLITES

Je. Vovchyk[1], Ja. Blagodyr[1], F. Masumi[2], and N. Bakhtigarajev[2]

[1] *Astronomical Observatory, Ivan Franko National University, Lviv, Ukraine*
e-mail: `eve@astro.franko.lviv.ua`

[2] *INASAN RAS, Moscow, Russia*
e-mail: `nail@osiris.inasan.rssi.ru`

Identification of satellites is the complicated problem. One of the possible way to solve this problem is a determination of orbit of the object. However, additional information is often necessary. Such information could be received from the electrophotometric observations of satellites. The Lviv Astronomical Observatory and observation station of INASAN RAS (Zvenigorod Astronomical Observatory) have instruments for such a type of observations.

INTRODUCTION

In the last decades the problem of "cosmic debris" has became very actual. A quantity of artificial satellites and debris in cosmos are increasing in time. Therefore, observations and identifications of all the bodies flying in near Earth space were conducted at the Astronomical Observatory, Ivan Franko National University of Lviv, Ukraine (LNU), and at the Zvenigorod Observatory of Astronomical Institute of RAS, Moscow, Russia (ZO). These institutions are engaged in the works on photometric observations of the low orbit objects.

INSTRUMENTS FOR ELECTROPHOTOMETRIC OBSERVATIONS OF ARTIFICIAL SATELLITES

As the base for making photometric observations ZO and LNU have used the mounting and optics of laser ranger systems (ZO – from the LD-3 and LNU – from LD-2). In LNU self-made electrophotometer with the two 34 cm objectives was mounted. The pulses from photomultipliers are transmitted to selection and operation processing block, where amplifying, discrimination and transformation of current-code during the integration time as well as transmission to IBM computer for saving and visualization take place. In parallel the pulses from quartz clock are supplied with an accuracy of 0.001 sec. Observations of the North Polar Sequence standard stars showed the penetrating ability of $9\overset{m}{.}97$ in filter V and $9\overset{m}{.}78$ in B. The TV-camera SIM-ICCD-05 as a light-receiver was used in ZO for photometric observations. The TV signal is transferred to a computer by special video card and than is processed and wrote to file. Penetrating ability for stars is $10\overset{m}{.}45$ and for fast moving objects (low-orbit satellites) is $9\overset{m}{.}2$ with optics of guide telescope of LD-3 (D=250 mm, D:F=1:5).

RESULTS OF PHOTOMETRIC OBSERVATIONS

Various satellites were observed and light-curves were obtained with the described electrophotometer of LNU and TV-photometer of ZO. They were – Ajisai, Topex, GFO, Ers-1, Ers-2, Cosmos-2344, Geos-3, Spot-1, Spot-2, Spot-4, 92083 A, 95066 A, 96072 A, and others. As a rule the photometric observations were made for the objects with known orbital data and shapes. So, they are not real "space debris". But observations of satellites with a priori known shapes give the possibility to compare some details of experimental light-curves with details on surfaces of the objects and make the first step for solving the reverse problem – to define the shape of the object from its light-curve. As examples of the obtained light-curves, the light curves of the Topex satellite observed at LNU and at ZO are demonstrated in Fig. 1 and Fig. 2, respectively. In ZO the changes of period of rotation of some satellites were analysed. For the Cosmos-2344 satellite the rotating period has changed from 71.58 seconds in 1998 to 94.66 seconds in 1999.

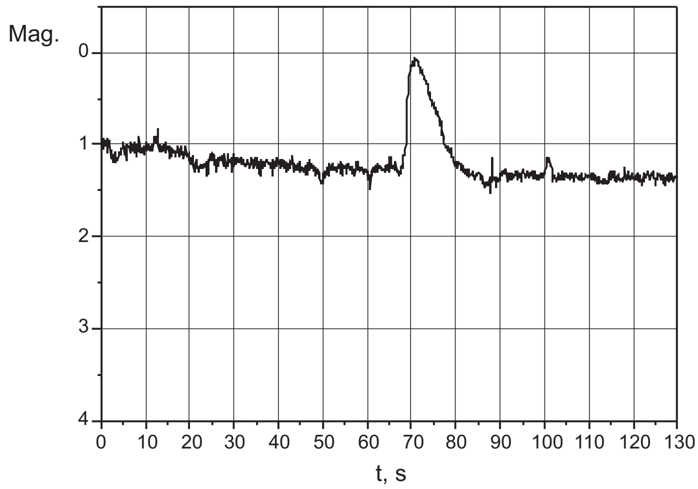

Figure 1: The light-curve of the TOPEX satellite in filter V received on May 9, 1999 in the LNU at 19:35 UT. The location of the satellite, observer and Sun is such that it gives a flash on the curve

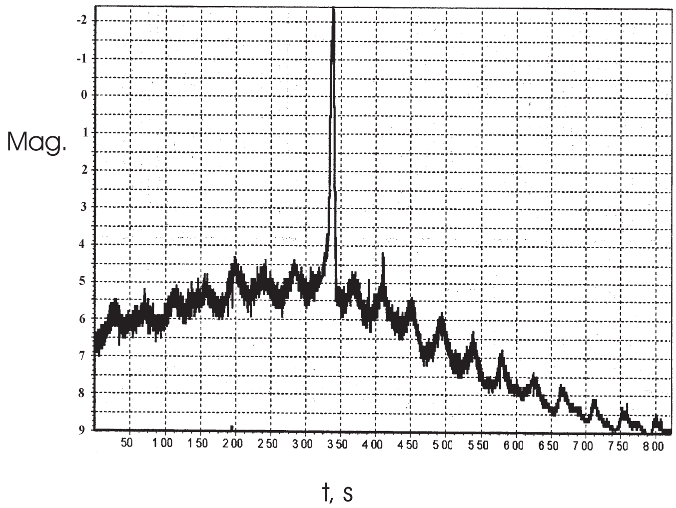

Figure 2: The light-curve of the satellite 97028 obtained at the ZO on April 17, 1999 at 22:42–22:58 UT. A flash produced by solar-panel is well seen

CONCLUSIONS

The photometric observations are one of the ways, which allows to get an additional information about a behaviour of object on orbit and its shape. It is important part of work when solving the problem of space debris.